# CMB Foreground and separation methods

Astro 448
Yuxi Zhao
12/5/2018

# Outline

- CMB foreground overview
  - Thermal Dust
  - AME (spin dust, spinning nanodiamonds? )
  - Synchrotron
  - Free-free
  - CO
  - Zodiacal light, CIB
- Component separation methods
  - Template fitting
  - Parametric method: Commander
  - Non-parametric methods: NILC, FastICA, SMICA,ABS

# Various types of foregrounds

Dickinson, 2016

| Foreground | Polarization | Angular scales | Mitigation technique |
|---|---|---|---|
| Atmosphere | $\approx 0\,\%$ | Large scales | Space/Balloon/high altitude sites |
| Ground | Varies | Large scales | Space/ground shield/low beam sidelobes |
| Radio Freq. Interference (RFI) | $0-100\,\%$ | All | Space/remote sites/ground shield |
| Sun/Moon | Low | All | Space/low beam sidelobes |
| Planets/solar system objects | Low | Small scales | Low frequencies / high resolution |
| Zodiacal light | Low | Large scales | Low frequencies |
| Galactic synchrotron radiation | $\approx 10-40\,\%$ | Large scales | Spectrum/high freqs. |
| Galactic free-free radiation | Low | Large scales | Spectrum/H$\alpha$/recomb. lines |
| Galactic thermal dust radiation | $\approx 2-20\,\%$ | Large scales | Spectrum/low freqs/starlight abs. |
| Galactic spinning dust radiation | Low | Large scales | Spectrum/FIR templates |
| Galactic magnetic dust radiation | $0-35\,\%$ | Large scales | Spectrum |
| Galactic line emission (e.g. CO) | Low | Large scales | Narrow bandpasses |
| Radio galaxies | Few % | Small scales | High frequencies/high resolution |
| Sub-mm/IR galaxies | Low | Small scales | Low frequencies/high resolution |
| Infrared Background (CIB) | Low | Small/interm. scales | Low frequencies/very high resolution |
| Secondary Anisotropies | Low | All | Spectrum/spatial |

# What does foregrounds look like?

# Temperature maps

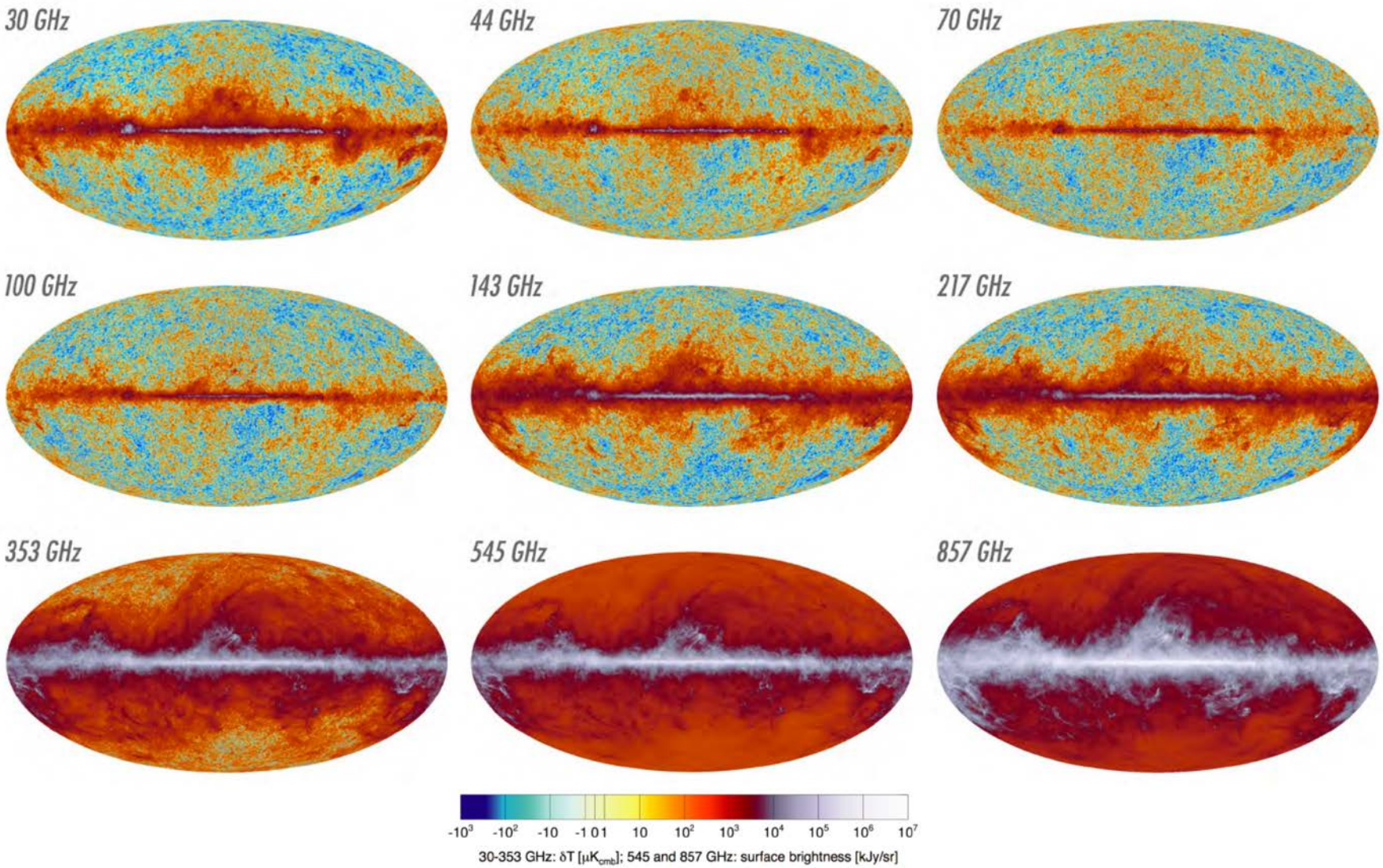


Planck 2015 results. I

# What does foregrounds look like?

# Polarization maps

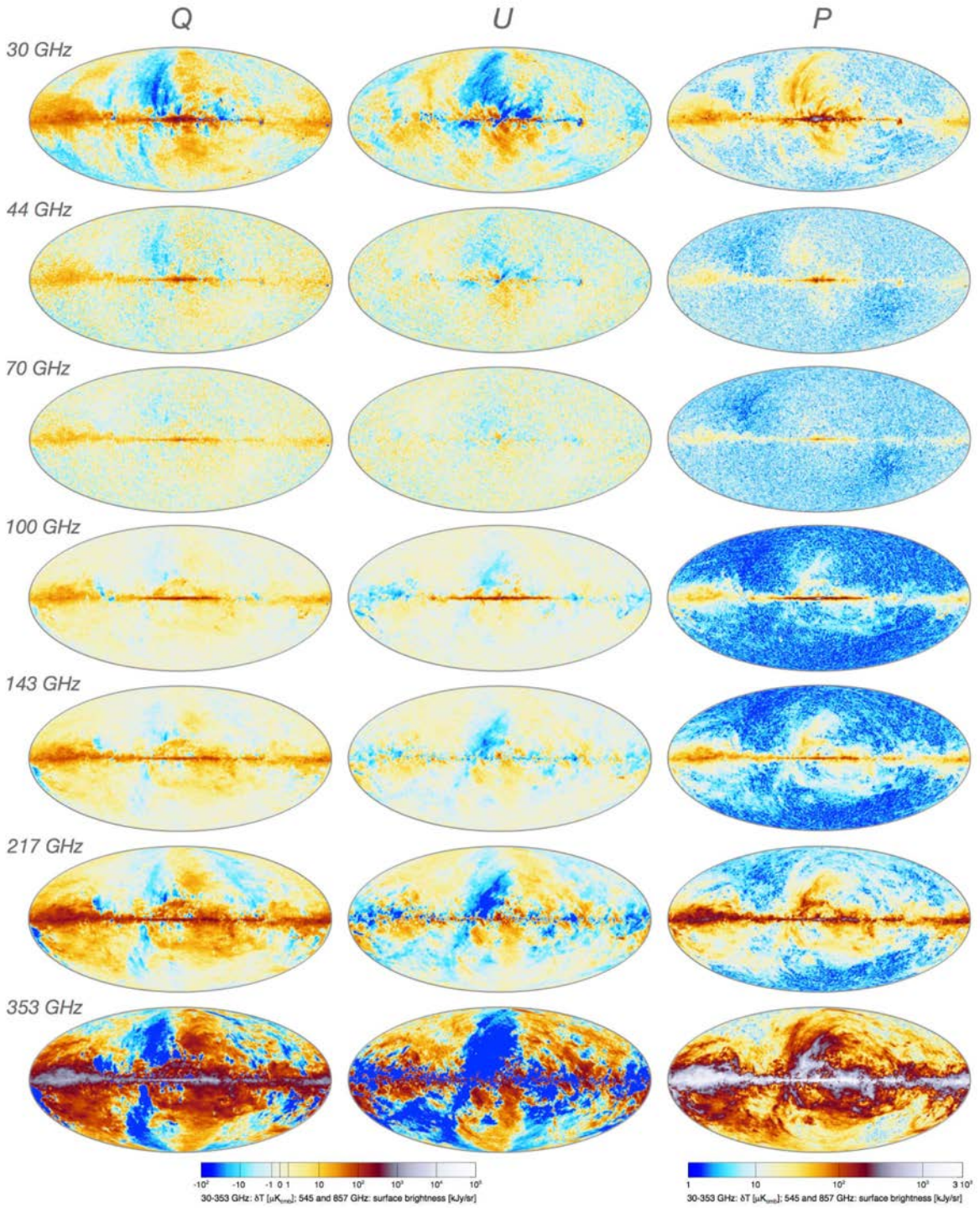


An intuitive conclusion:

Galactic component dominate the foreground.

Polarization fraction:

$$\Pi = \frac{P}{I}$$

Planck 2015 results. I

# Spectral characteristics of foregrounds and CMB

temperature

polarization

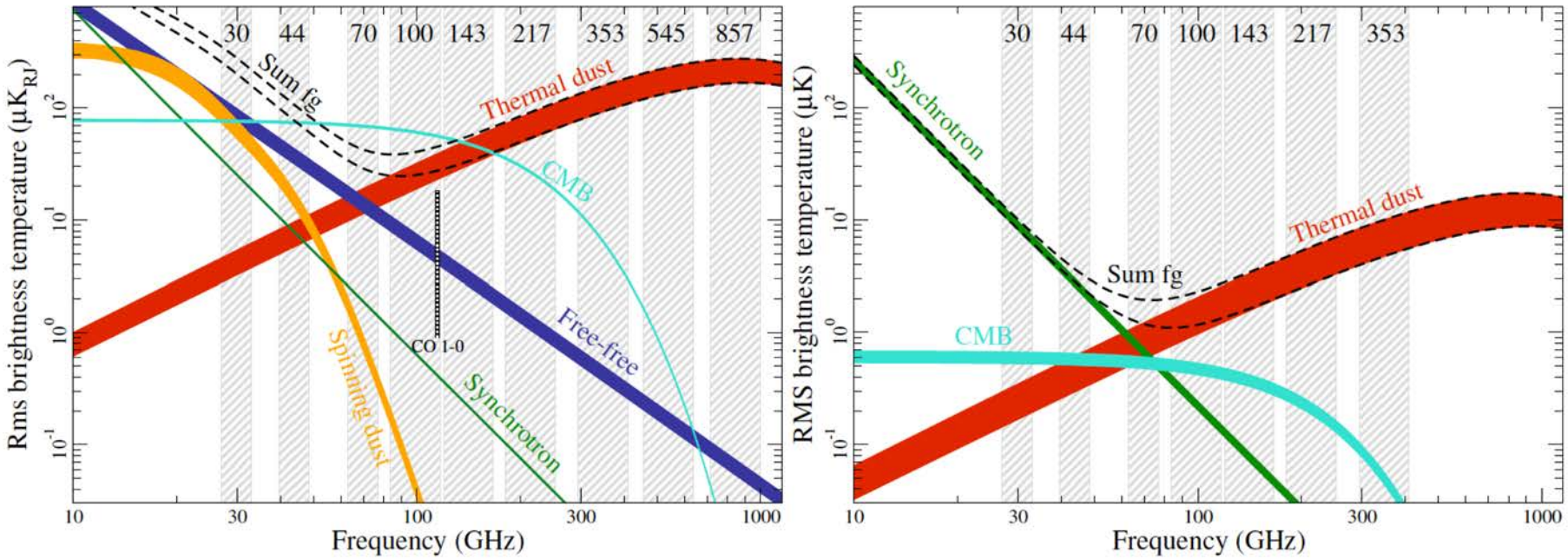


Planck 2015 results. I

- Galactic radiation are most notably foregrounds, and dominating at the lower and higher frequencies.
- The foreground minimum is at 70 GHz
- The foregrounds in temperature are more complex but the brightness is acceptable
- While in polarization, the situation is quite on the contrary

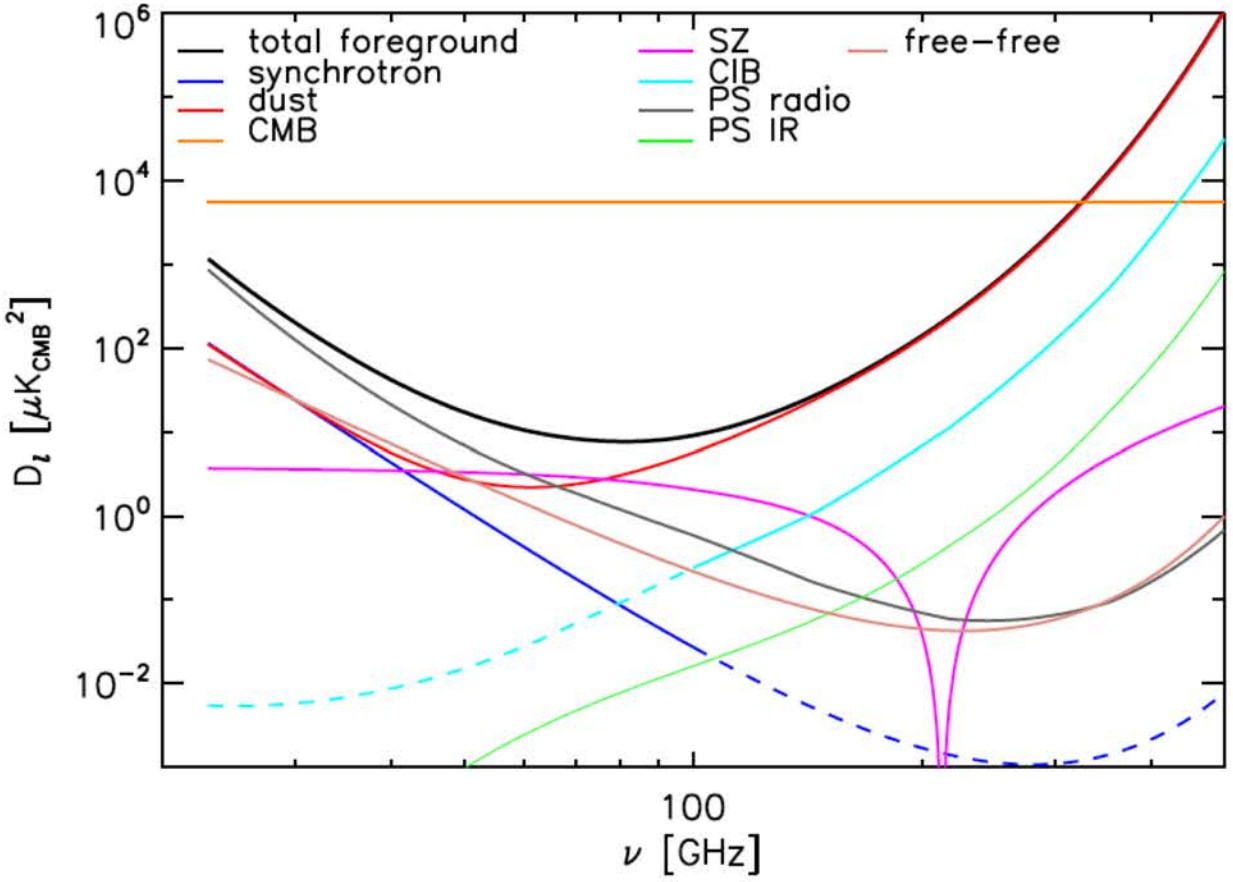


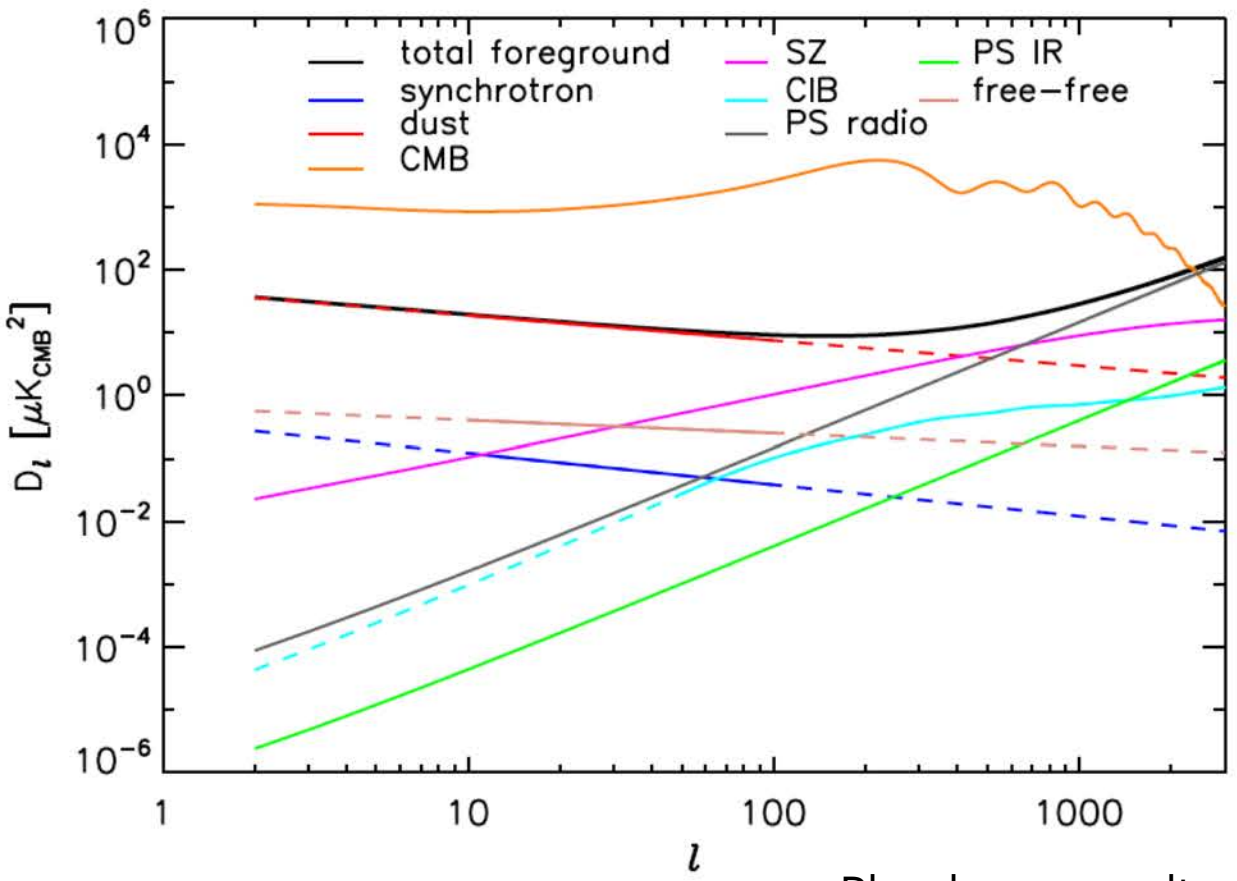


Planck 2013 results. I

# Power spectrum of foreground

- Left: frequency spectra, $l = 200$ ( first peak )
- Right: angular power spectra, $\nu = 100GHz$
- Solid lines show where the spectra are estimated from data, and dashed lines are extrapolations

# Thermal dust

# gray body

- At frequencies 70 GHz, thermal emission from the interstellar dust grains mostly made of graphites, silicates, and PAHs (Polycyclic Aromatic Hydrocarbons) dominates the foreground.
- Blackbody emission modified by opacity effects, which is a modified blackbody spectrum

- $T(\nu) = \tau_{\nu_0} \left(\frac{\nu}{\nu_0}\right)^{\beta_d} B(\nu, T_d)$
- $\beta_d$ : emissivity index
- $\tau$ : dust optical depth

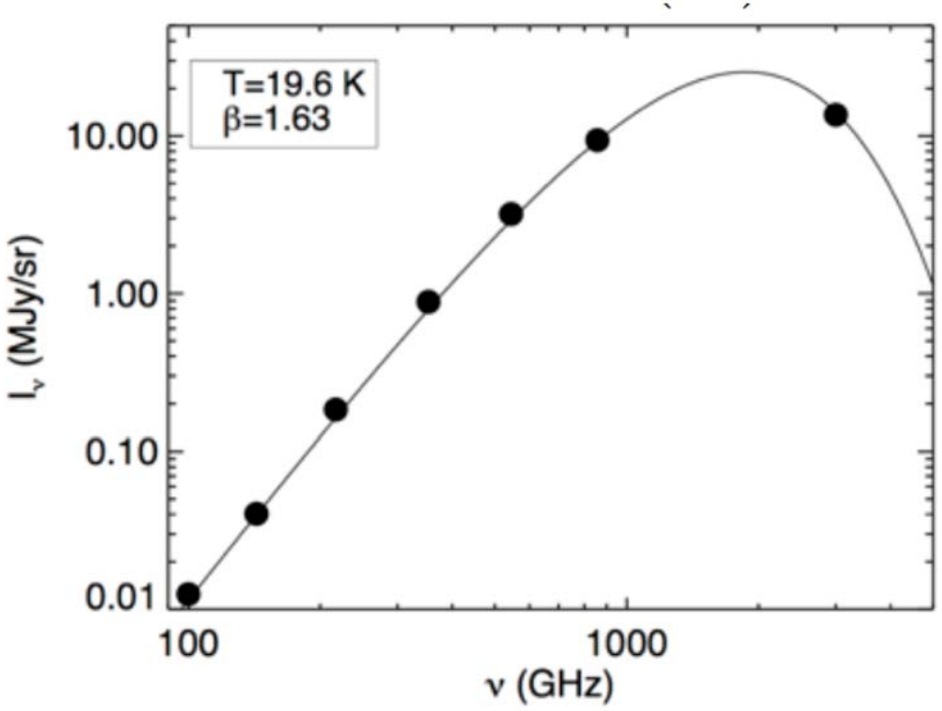


Planck 2013 results XI

# Thermal dust

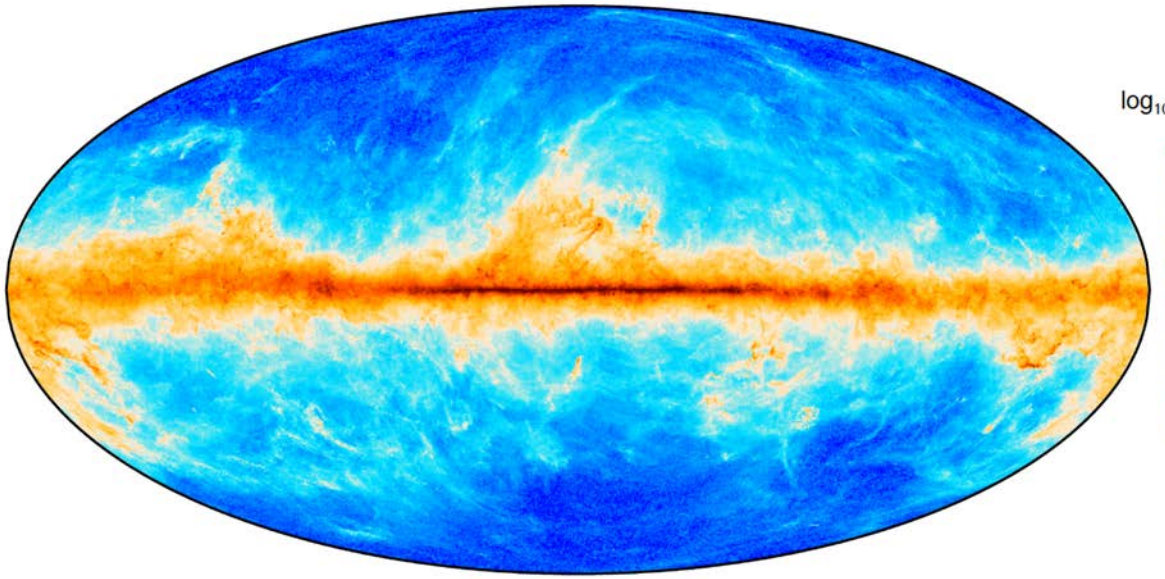


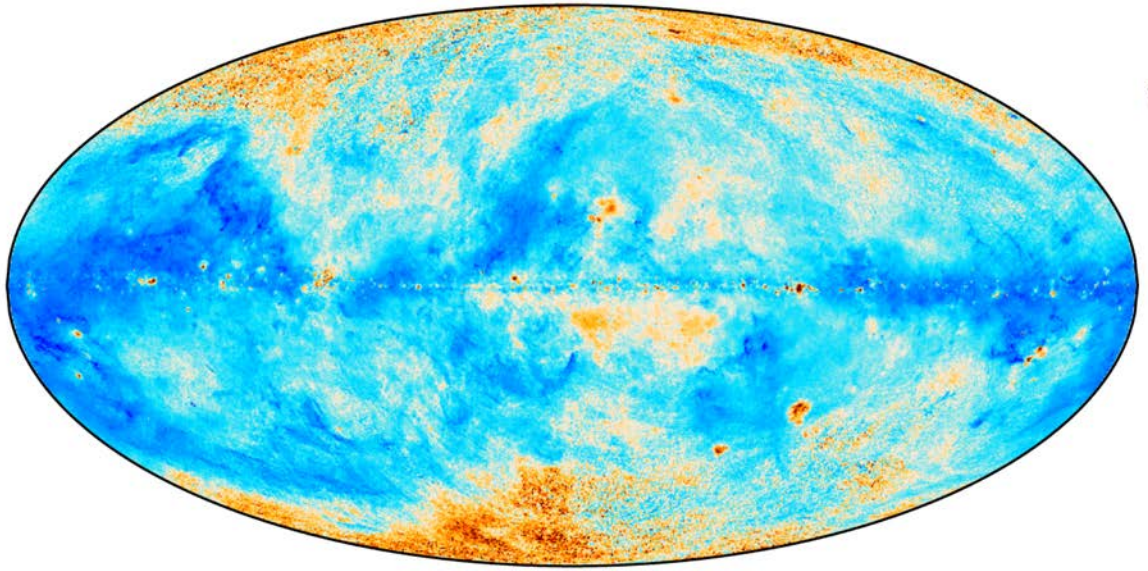


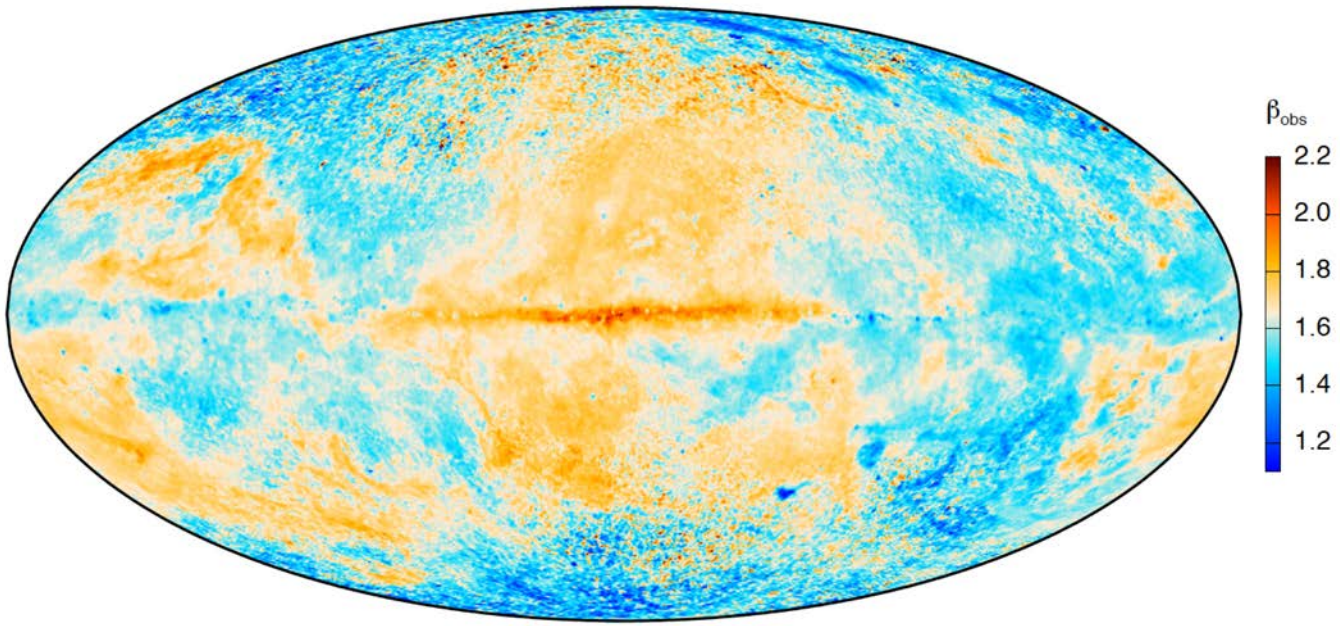


Planck 2013 results. XI.

# Thermal dust

# two-component model

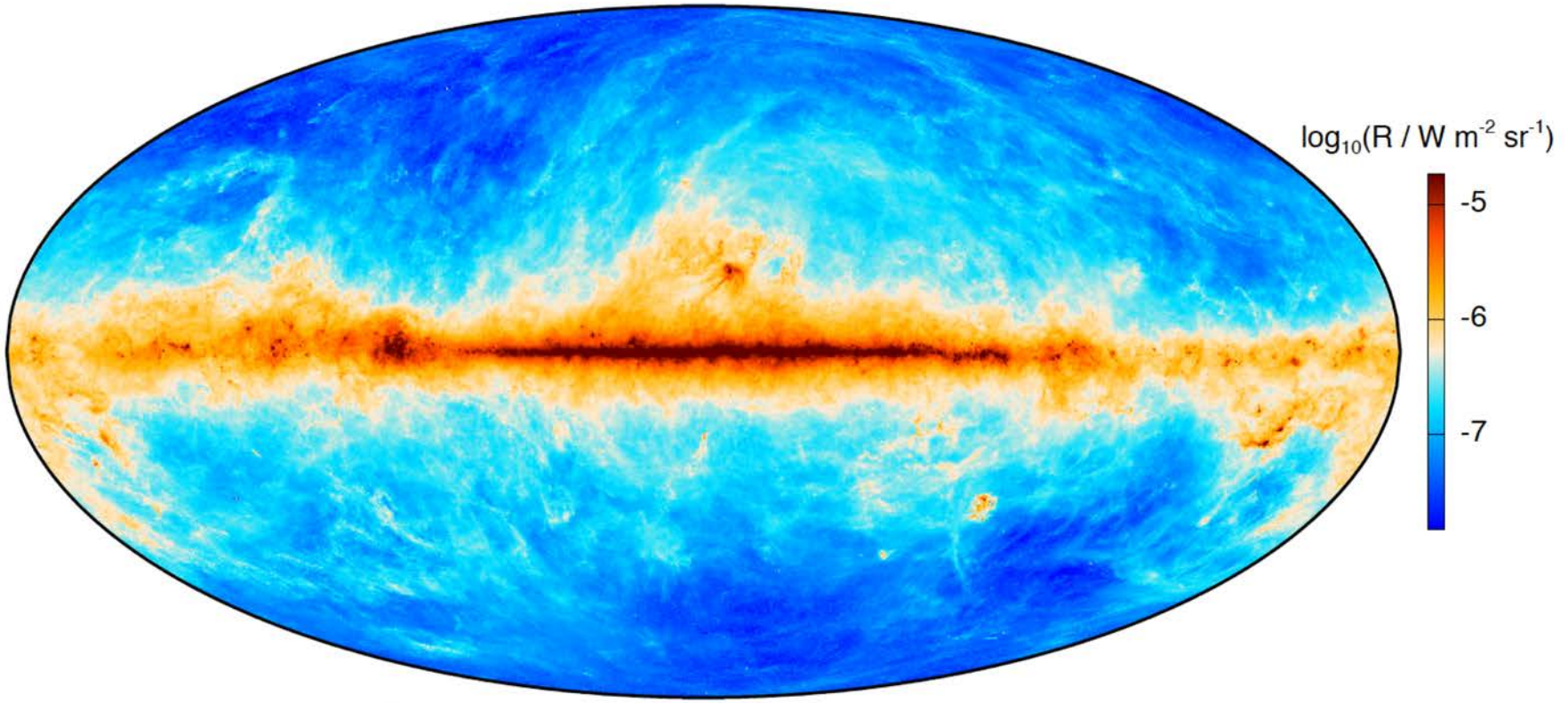


Planck 2013 results. XI.

- Dust radiance $\mathcal{R} = \int_{\nu} I_{\nu}\, \mathrm{d}\nu.$
- Single-component model may introduce systematic errors at lower frequency.
- Different-sized grains intrinsically require multicomponent model.
- Famous SFD dust model (*Schlegel, Finkbeiner & Davis, 1998*) :

  two components $T_{1,2} = (9.4, 16)K$ , $\beta_{1,2} = (1.67, 2.70)$

# Thermal dust polarization

- Grains will emit (or absorb) photons most efficiently along the shortest axis.
- Long grain axis tend to align by the local magnetic fields.
- So the polarization is perpendicular to magnetic fields.
- Degree of alignment rely on the size of grain, leading to frequency-dependent polarization.

$$Q_\nu^{dust} = f_d\, g_d I_\nu \cos(2\gamma_d)$$
$$U_\nu^{dust} = f_d\, g_d I_\nu \sin(2\gamma_d)$$

A large fraction of the sky has polarization fractions > 5 %

At high latitudes, thermal dust polarized up to 20%

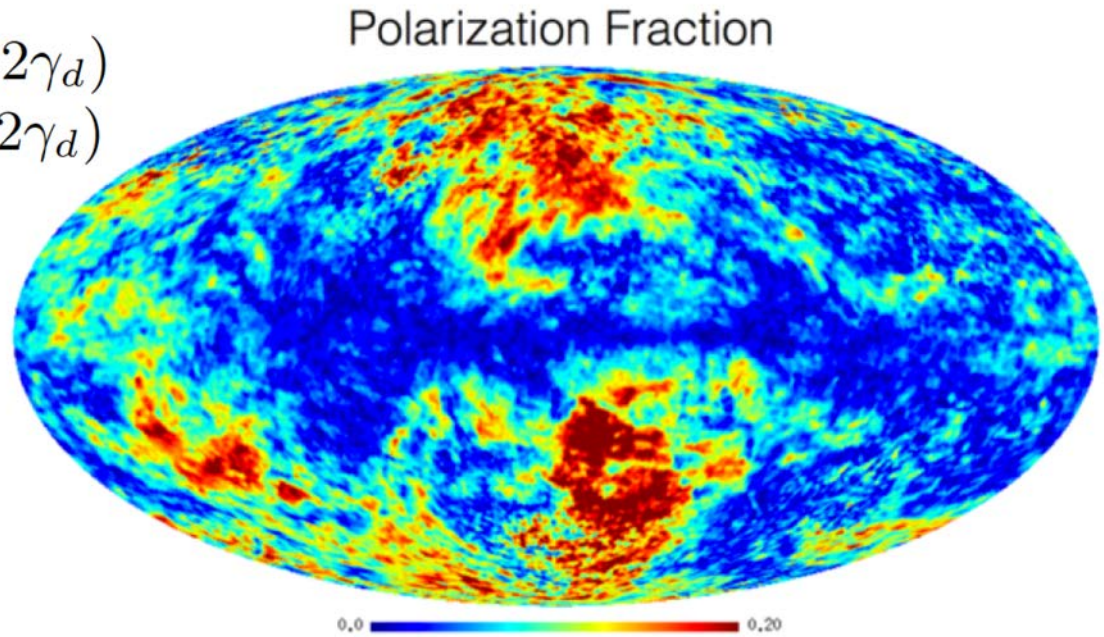


Planck intermediate results. XIX.

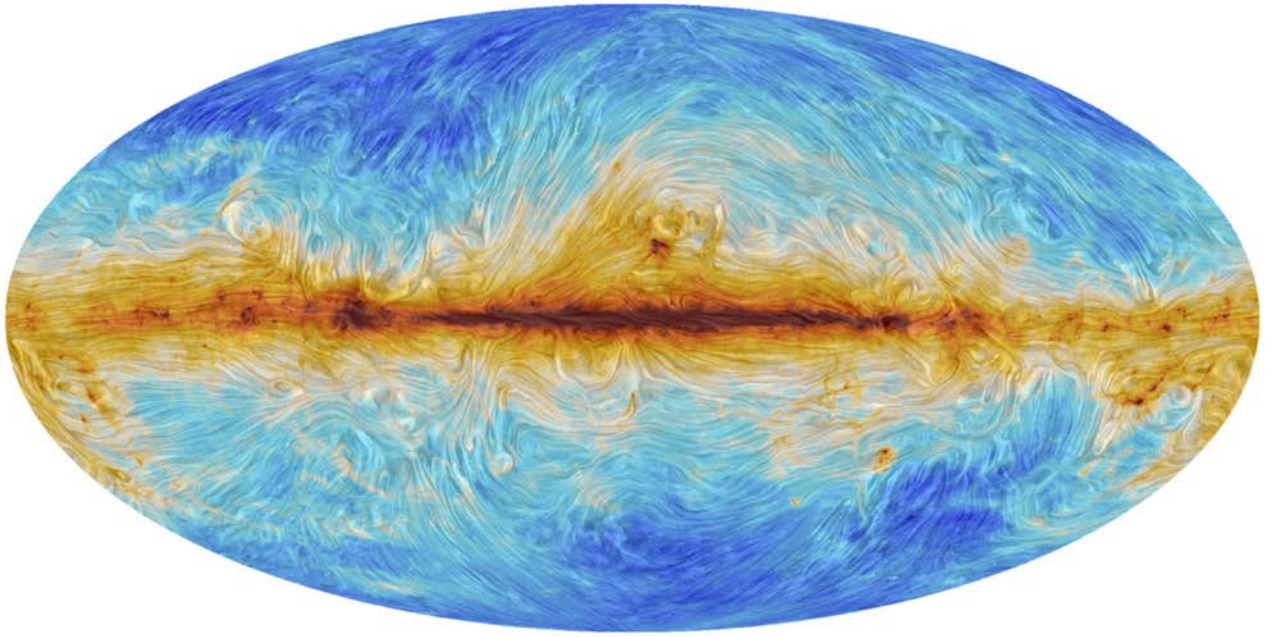

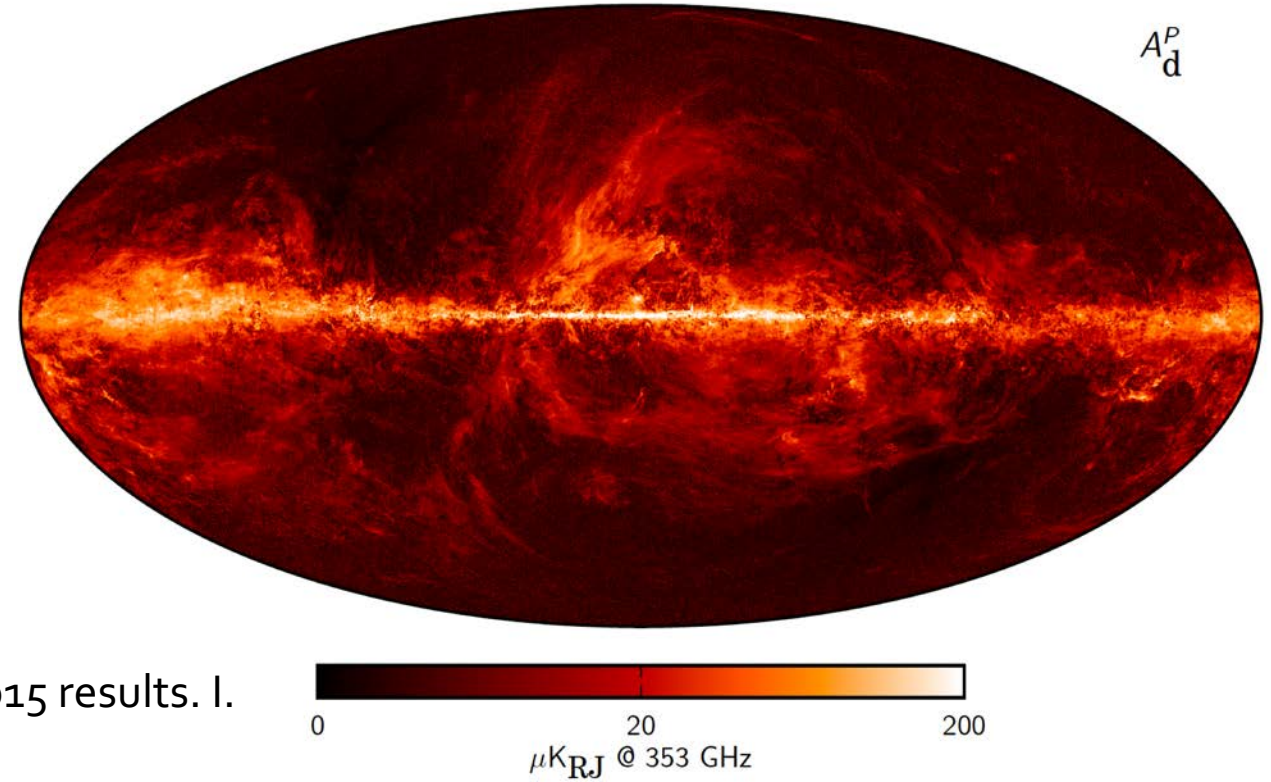


Planck 2015 results. I.

# Thermal dust polarization

- Left: angle of polarization at 353 GHz, rotated by 90° to indicate the direction of the Galactic magnetic field projected on the plane of the sky
- Right: dust polarization amplitude map, $P = \sqrt{Q^2 + U^2}$, at 353 GHz

# E mode, B mode angular power spectrum

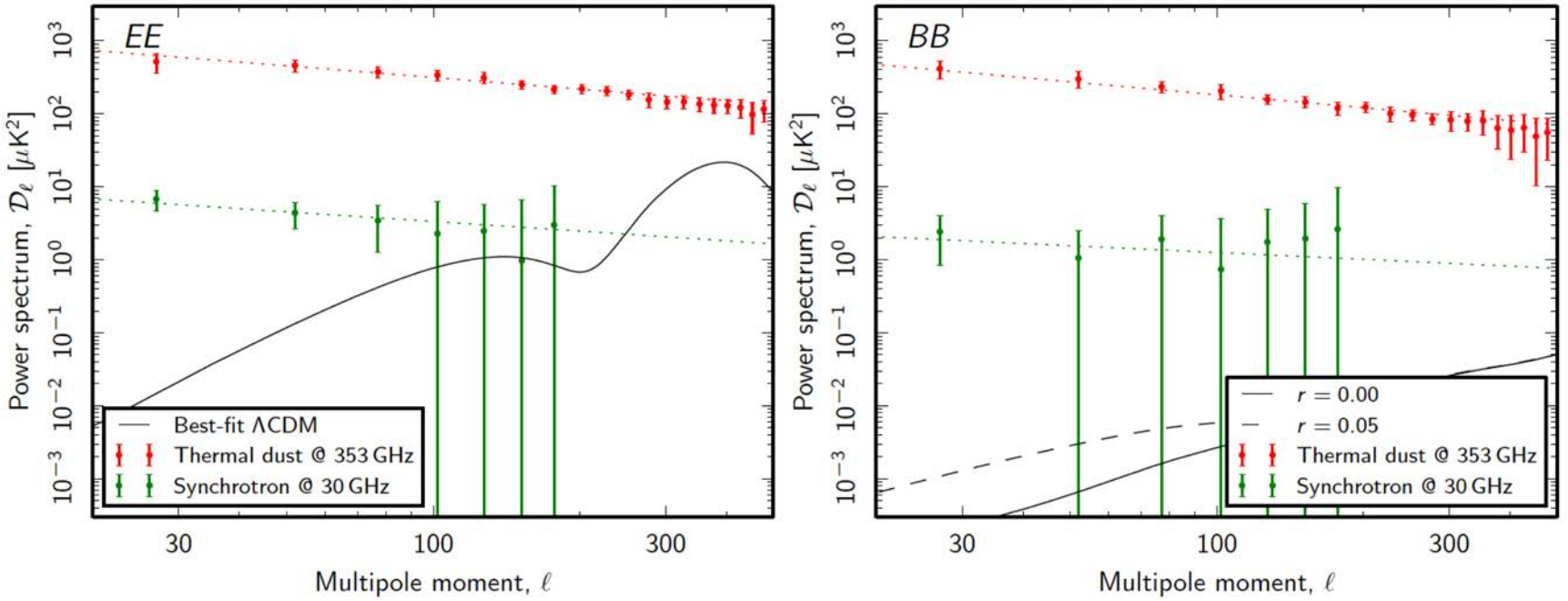


Planck 2015 results. X.

- The dashed lines: best-fit power-law models to each case
- The solid and dashed black lines: best-fit $\Lambda CDM$ power spectrum as fitted to temperature observations only
- r: tensor-to-scalar ratio
- B mode signal is really hard to extract !

# Spin dust

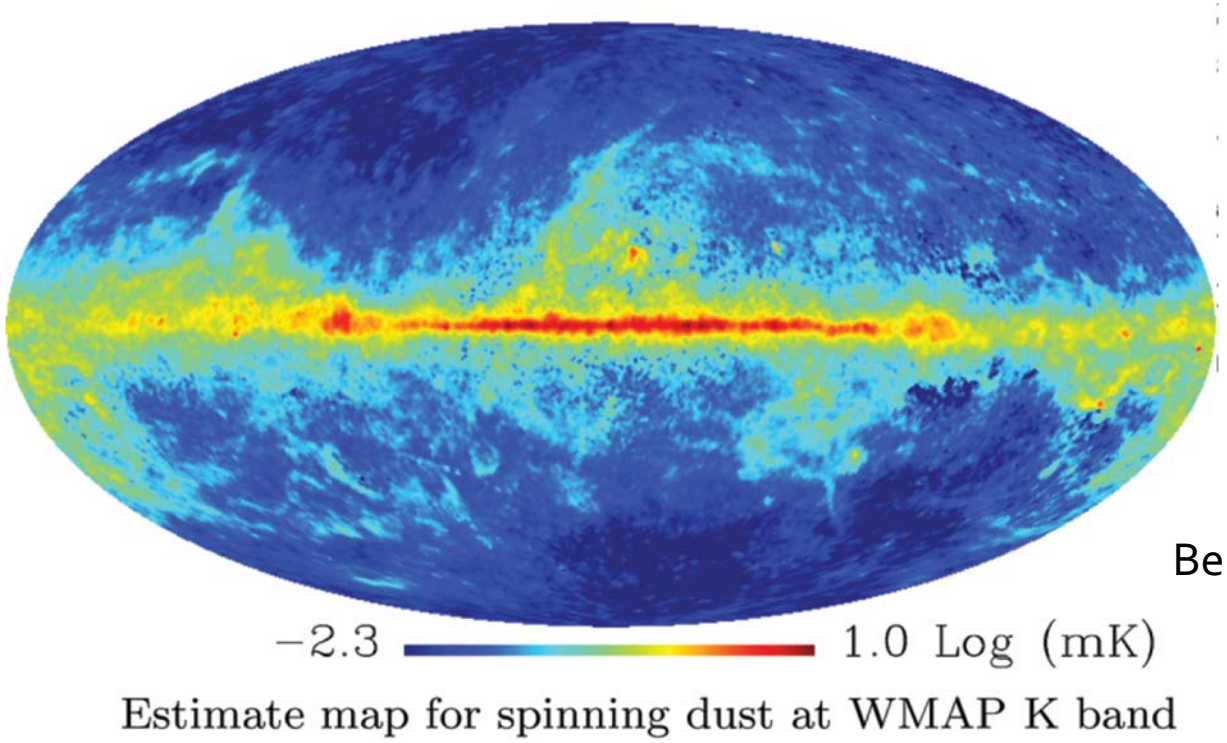


Estimate map for spinning dust at WMAP K band

Bennet et al. (2013)

- Anomalous emission at 20–60 GHz, firstly recognized as free-free, but lack of correlation with Hα line.
- Spatial distribution is closely related to the thermal dust.
- Spin dust emission: smallest ( $10^{-9}$ m) dust grains with electric dipole moment, they rotate at GHz frequencies.

# Spin dust

# two-component model

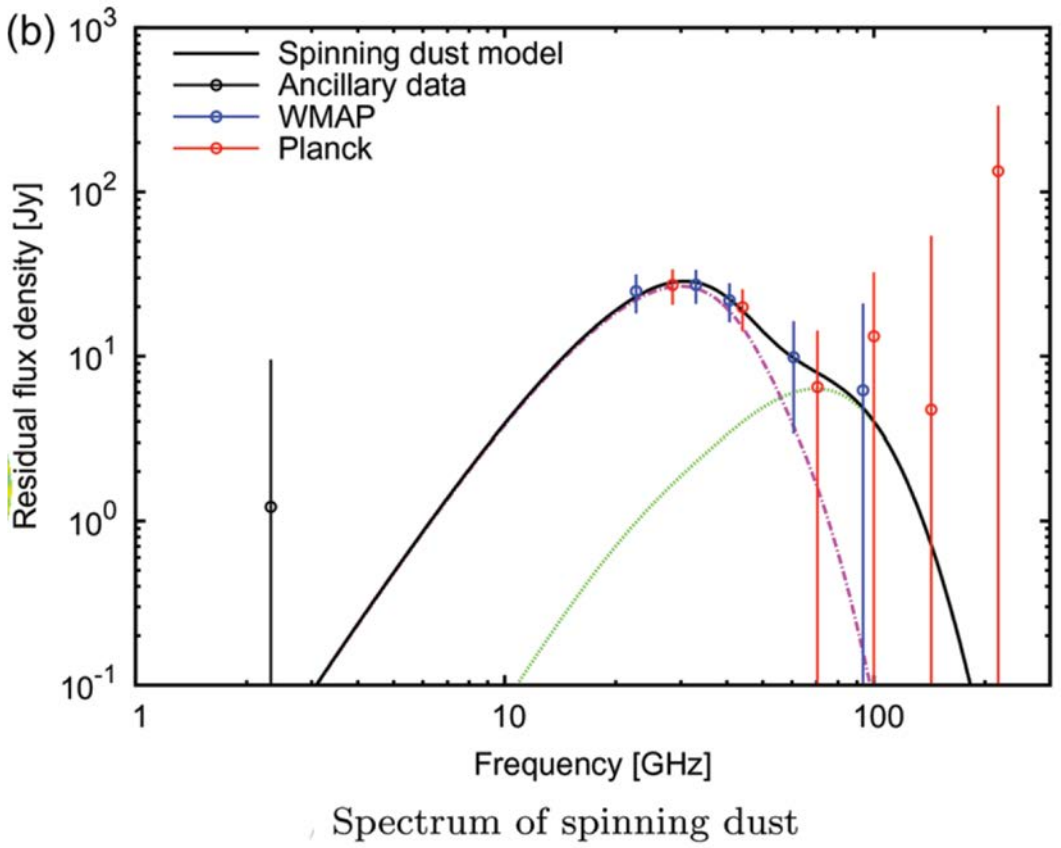


Planck collaboration et al. (2011)

- The anomalous emission spectrum is consistent with the spinning dust model of Draine et al. (1998)
- Two-component model : dense molecular gas and low-density atomic gas. *[ Ali-Haïmoud et al. 2009]*

# spin dust

- Spinning diamonds?

  Anomalous microwave emission from spinning nanodiamonds around stars, *Nature Astronomy* (2018).

- Polycyclic aromatic hydrocarbons (PAHs) used thought to be the candidate source of AME
- Found AME in three protoplanetary disk
- Both PAHs and nanodiamonds emit infrared light
- Other protoplanetary disks with infrared signature of PAHs show no signs of AME

# Synchrotron modeling

Synchrotron radiation is emitted by relativistic cosmic ray (CR) electrons, which are accelerated by the Galactic magnetic field.

- CR Number density and energy spectrum, $N(E) = KE^{-p}$
- Strength of the magnetic field, $B$
- Spatial dependence

- Spectrum of antenna temperature $\mathrm{T}(\nu) \propto B^{\frac{p+1}{2}} \nu^{\beta}$ , where $\beta = -\frac{p-1}{2}$. *[G. B. Rybicki and A. P. Lightman, Radiative Processes in Astrophysics]*

Full-sky realization model:

- Haslam et al. (1982) map at 408 MHz, used by WMAP
- map at 1.4 GHz by Reich and Reich (1986)
- Global Sky Model (GSM) by de Oliveira-Costa et al. (2008)
- GALPROP model, Orlando & Strong (2013 ), used by Planck

# Synchrotron modeling

- Larmor formula

$$P_{\rm e} = P'_{\rm e} = \frac{2e^2}{3c^3}\left[a'^2_{\parallel} + a'^2_{\perp}\right] = \frac{2e^2}{3c^3}\gamma^4\left[\gamma^2 a^2_{\parallel} + a^2_{\perp}\right]$$

- only acting force is the (relativistic) Lorentz force

$$F_{\rm L\parallel} = e\,v_{\parallel}B = 0 \quad \rightarrow \quad a_{\parallel} = 0$$

$$F_{\rm L\perp} = \gamma m\frac{dv_{\perp}}{dt} = e\,\frac{v_{\perp}}{c}B \quad \rightarrow \quad a_{\perp} = \frac{evB\sin\theta}{\gamma mc}$$

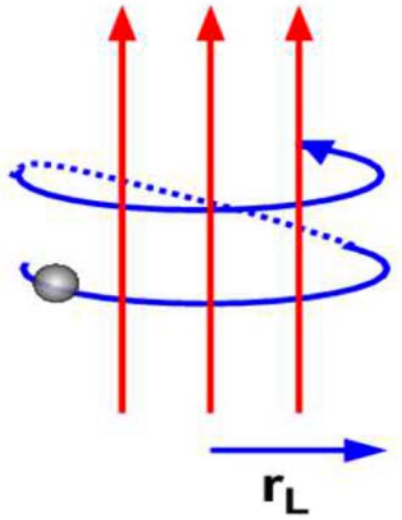


- Then we have the energy loss rate $P_{\rm S} = \frac{2e^4}{3m^2c^3}B^2\gamma^2\beta^2\sin^2\theta$

  Average over the solid angle

$$\langle P_{\rm S}\rangle = \frac{4}{3}\sigma_{\rm T}cU_B\gamma^2\beta^2$$

- Due to the beaming effect, some detailed calculation is needed to get the expression of it's power spectrum.

$$P_{\rm s}(\nu,\gamma,\theta) = \frac{\sqrt{3}e^3B\sin\theta}{m_{\rm e}c^2}F(\nu/\nu_c)$$

# Synchrotron modeling

$$P_s(\nu,\gamma,\theta) = \frac{\sqrt{3}e^3 B\sin\theta}{m_e c^2} F(\nu/\nu_c)$$

$$F(\nu/\nu_c) \equiv \frac{\nu}{\nu_c}\int_{\nu/\nu_c}^{\infty} K_{5/3}(y)dy$$

$$\nu_c \equiv \frac{3}{2}\nu_s \sin\theta$$

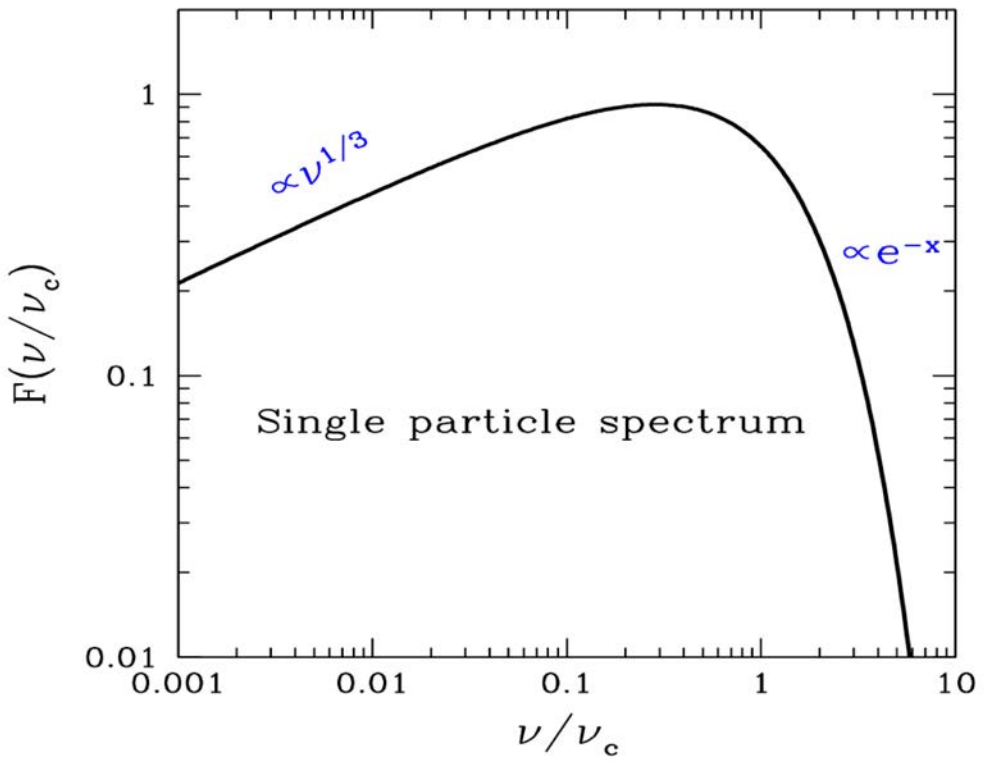


- For the emission from many electrons

$$\epsilon_s(\nu,\theta) = \frac{1}{4\pi}\int_{\gamma_{min}}^{\gamma_{max}} N(\gamma)P(\gamma,\nu,\theta)d\gamma$$

- emissivity is the power per unit solid angle produced within $1cm^3$

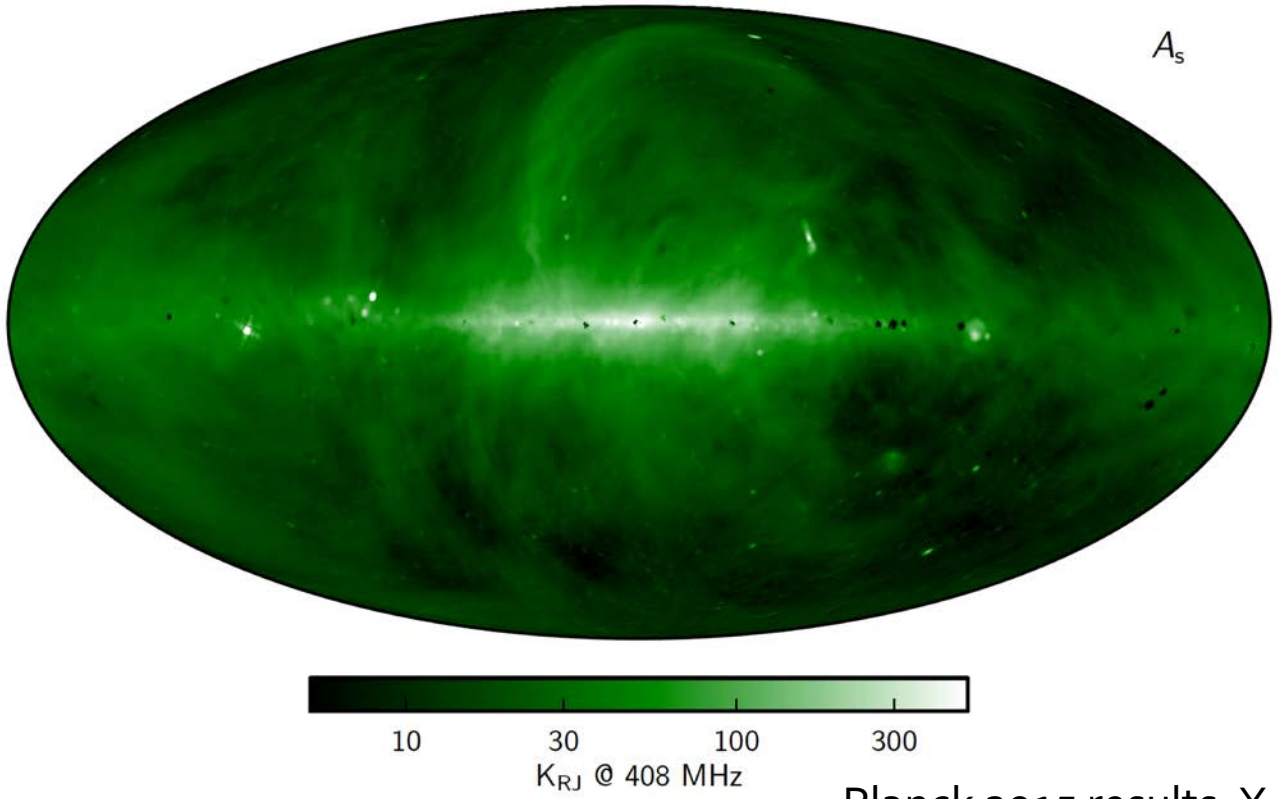


Planck 2015 results. X

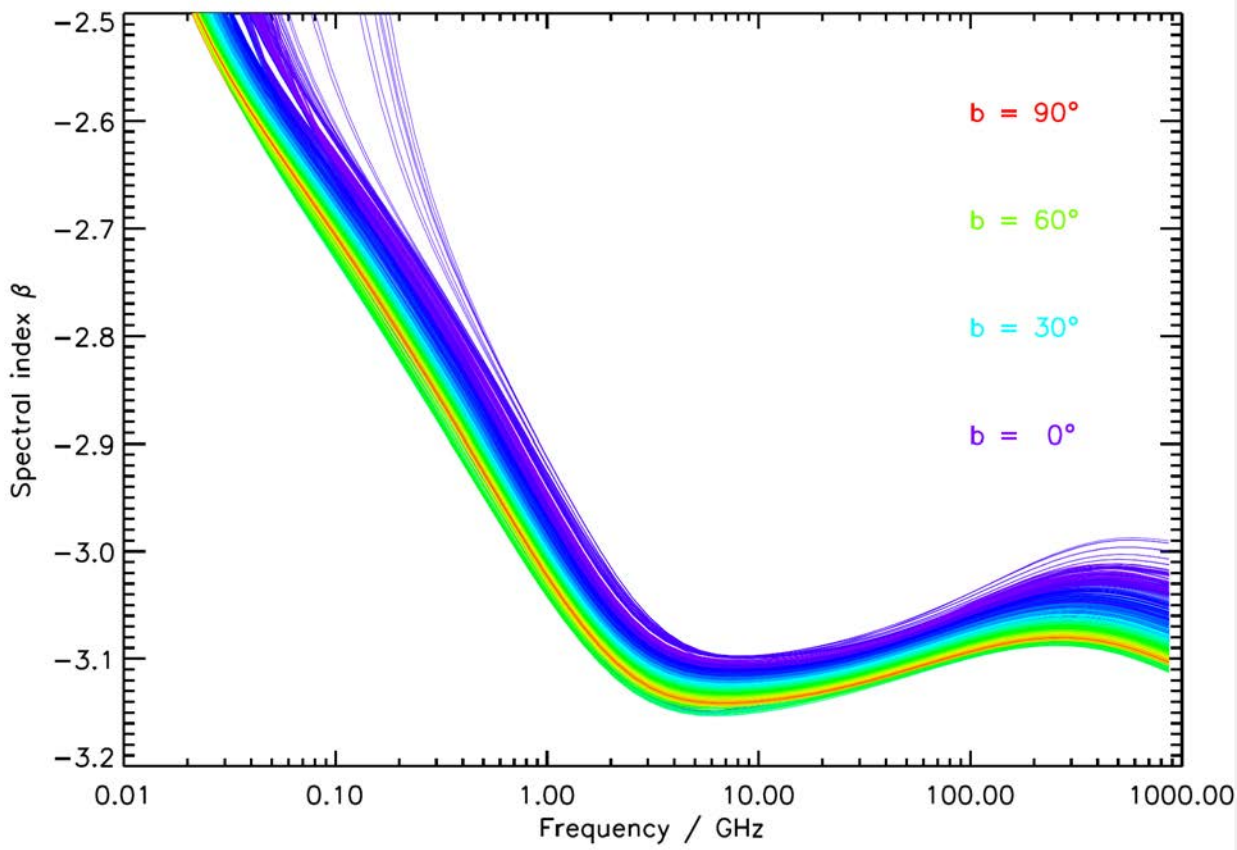


Planck 2015 results. XXV

# Synchrotron spectral index

- $b$ : Galactic latitude
- $\beta \approx -2.7$ at radio frequency
- Steeper values $\beta \approx -3.0$ around 10 GHz, spatial variation $\pm 0.2$
- Steepening: CR aging effect
- Flattening : multiple components

# Synchrotron polarization

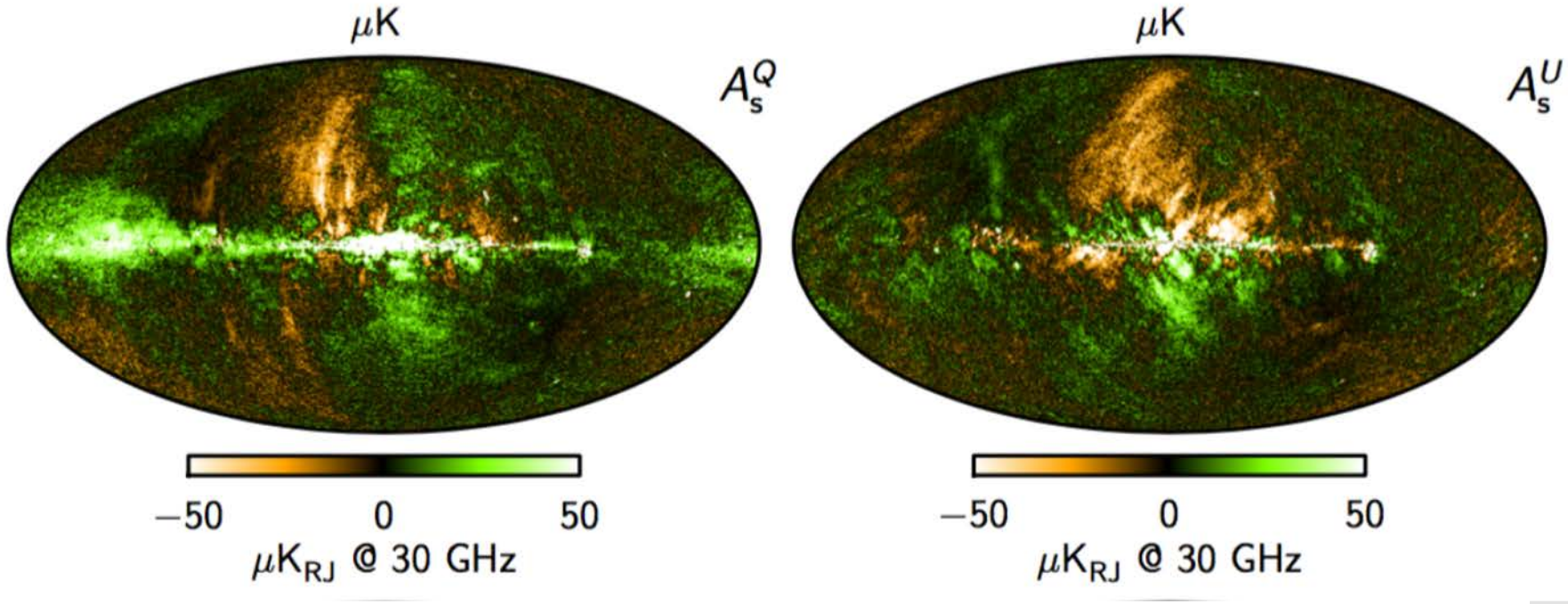


Planck 2015 results. X

- Polarized perpendicular to the magnetic field lines
- Degree of polarization $\Pi = (p+1)/(p+7/3)$
- Low frequency, low S/N, no accurate spectral index
- Simple power-law $\beta_s = 3$; or frequency dependence index, $C = \pm 0.3$ (Kogut et al. 2007)

$$Q_\nu^{sync} = Q_{23\,GHz}\left(\frac{\nu}{23}\right)^{\beta_s}$$

$$U_\nu^{sync} = U_{23\,GHz}\left(\frac{\nu}{23}\right)^{\beta_s} \qquad \beta_s(\nu) = -3 + C\log\left(\frac{\nu}{23}\right)$$

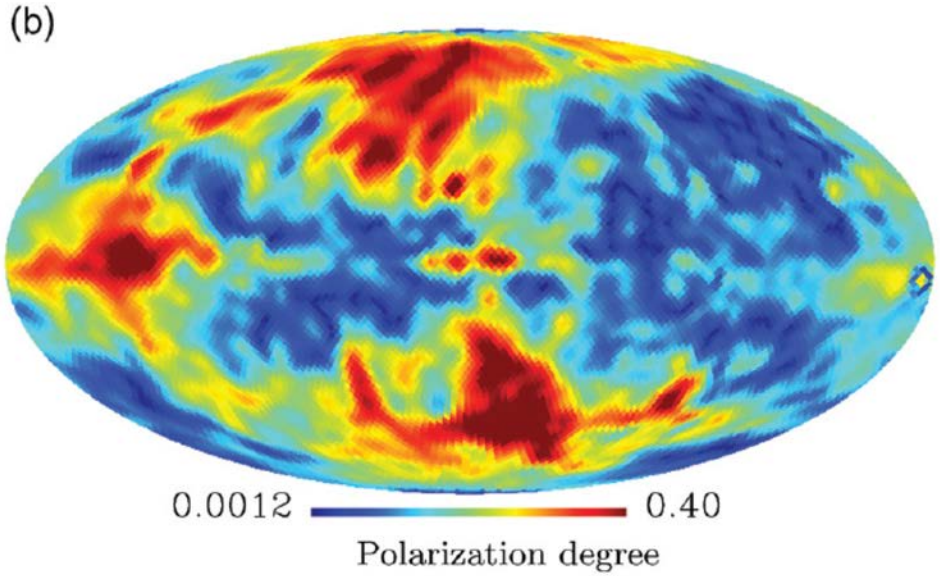


WMAP results. Gold et al.(2011)

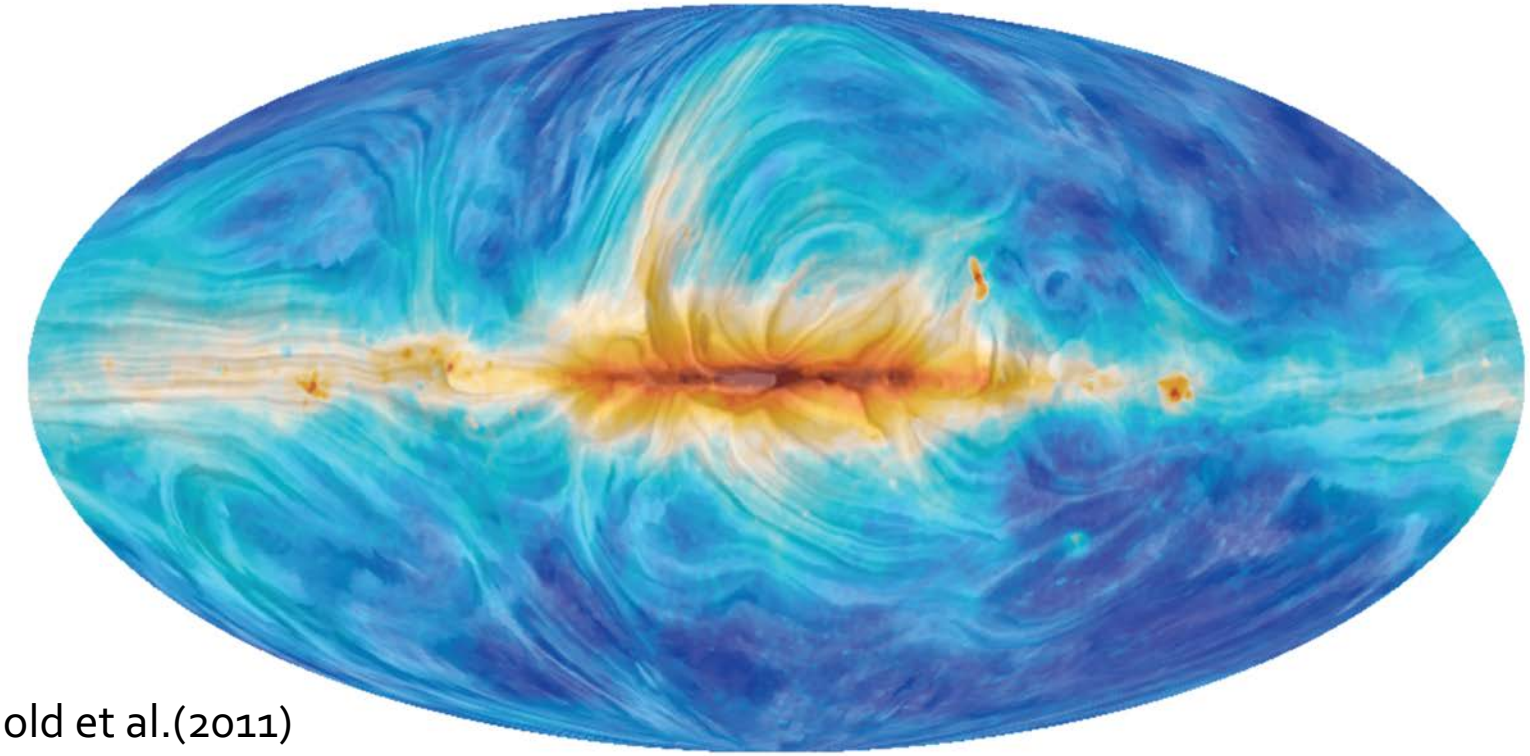

Planck 2015 results. I

# Synchrotron polarization

- Left: WMAP nine-years data, 23 GHz
- Right: angle of polarization at 30 GHz, dominated by synchrotron , indicate the direction of magnetic field,
- No precise polarization degree, but it's smaller at low latitude, because of superposition of different polarization angle

# Free-free

# derive the spectrum

- Free-free emission, also known as thermal bremsstrahlung, arises from electron–ion scattering in interstellar plasma.
- Intensity of free-free emission is given by an integration along the line of sight as $\mathrm{I}_\nu = \int j_\nu \, ds$, where $j_\nu$ is emissivity ( power radiated per unit frequency, per unit volume, per steradian)

$$j_{\mathrm{ff},\nu} = \frac{8}{3}\left(\frac{2\pi}{3}\right)^{1/2} g_{\mathrm{ff},i}\, \frac{e^6}{m_e^2 c^3}\left(\frac{m_e}{kT}\right)^{1/2} \mathrm{e}^{-h\nu/kT} n_e Z_i^2 n_i$$

- Gaunt factor:

$$g_{\mathrm{ff}} \approx \frac{\sqrt{3}}{\pi}\left[\ln\frac{(2kT)^{3/2}}{\pi Z_i e^2 m_e^{1/2}\nu} - \frac{5\gamma}{2}\right] \approx 6.155\,(Z_i\nu_9)^{-0.118}\, T_4^{0.177}$$

- For $h\nu \ll kT$, only Gaunt factor is frequency dependent

$$j_{\mathrm{ff},\nu} \approx 3.35\times10^{-40} Z_i^{1.882} n_i n_e \nu_9^{-0.118} T_4^{-0.323}\ \mathrm{erg\,cm^3\,s^{-1}\,sr^{-1}\,Hz^{-1}}$$

- Observed intensity $I_\nu$ is often expressed in terms of brightness temperature:

  $T_B = \frac{c^2}{2k\nu^2} I_\nu$
- $\Rightarrow T_B \propto \nu^{-2.12}$
- *[Bruce T. Draine, Physics of the Interstellar and Intergalactic Medium]*

# From bremsstrahlung to black body

- Free–free absorption, using the Kirchoff law

$$\alpha_\nu^{\rm ff} = \frac{j_\nu}{B_\nu} = \frac{4}{3}\left(\frac{2\pi}{3}\right)^{1/2} \frac{Z^2 n_{\rm e} n_{\rm i} e^6}{h m_{\rm e}^2 c^2} \left(\frac{m_{\rm e} c^2}{kT}\right)^{1/2} \frac{1 - e^{-h\nu/kT}}{\nu^3} \bar{g}_{\rm ff}$$

- At Raleigh–Jeans limit $\alpha_\nu^{\rm ff} = 0.018 \frac{Z^2 n_{\rm e} n_{\rm i}}{T^{3/2}\nu^2} \bar{g}_{\rm ff}$

- Source function (which is tend to be $I_\nu$ at optical thick case): $S_\nu \equiv \frac{j_\nu}{\alpha_\nu}$

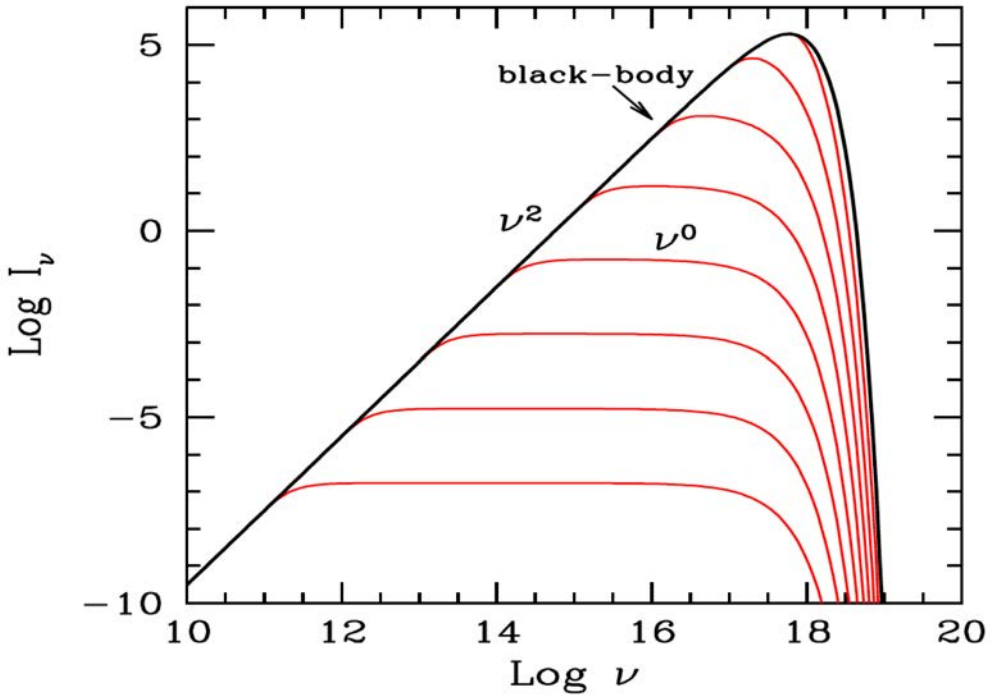

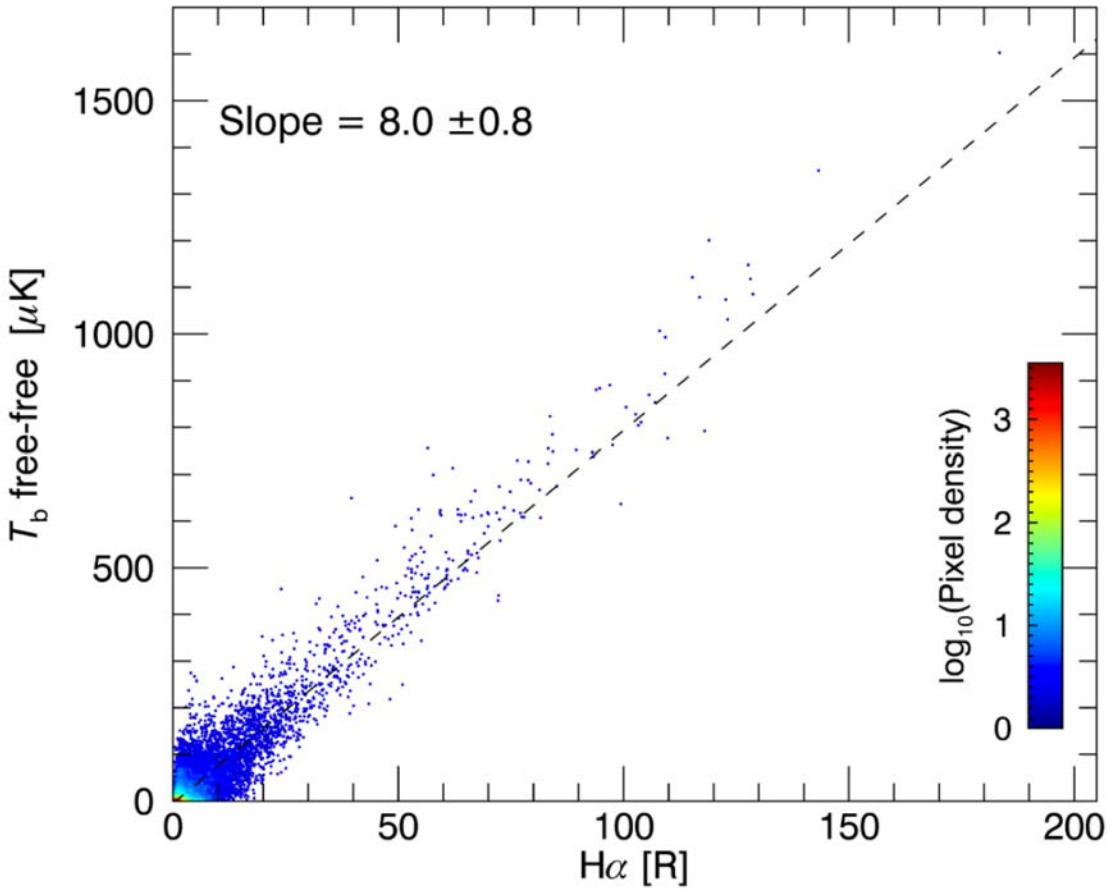


Planck 2015 results. XXV

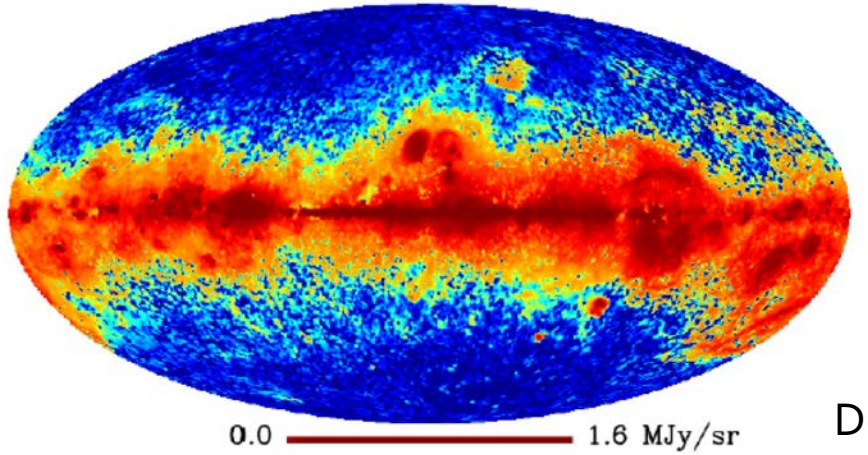


Delabrouille et al. (2013)

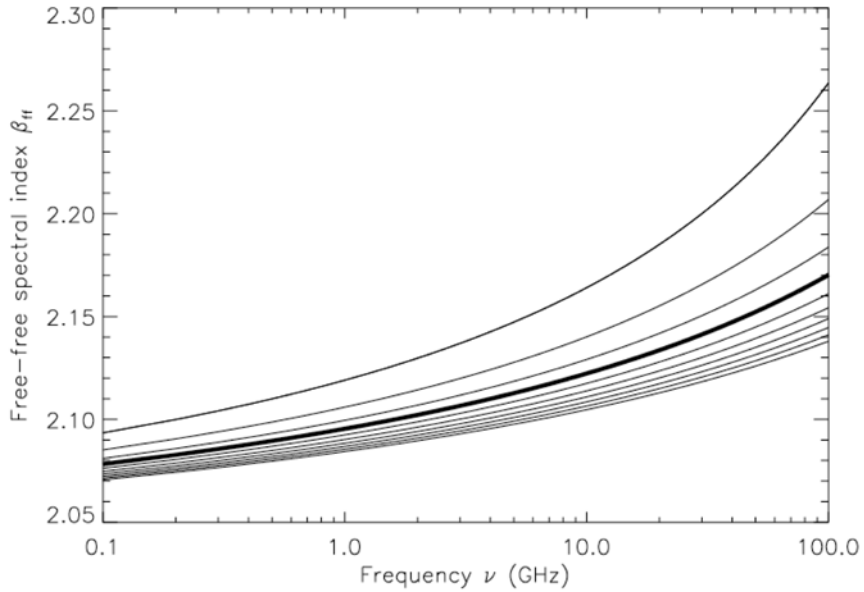


Dickinsion et al.(2003)

# Free-free

- The close correlation with the optical $H\alpha$ line, at 22.8 GHz
- At high Galactic latitudes, free-free emission is relatively weak
- At higher frequencies, the spectrum steepens slightly

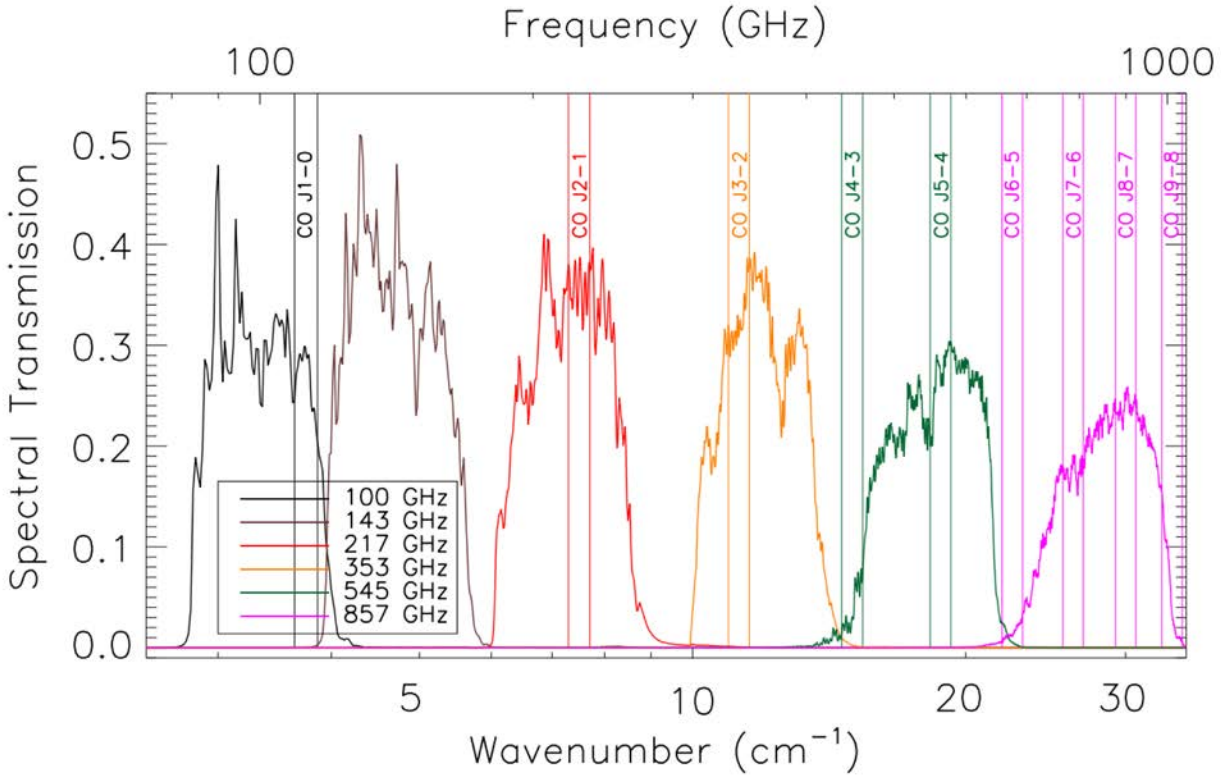


Planck early results. VI.

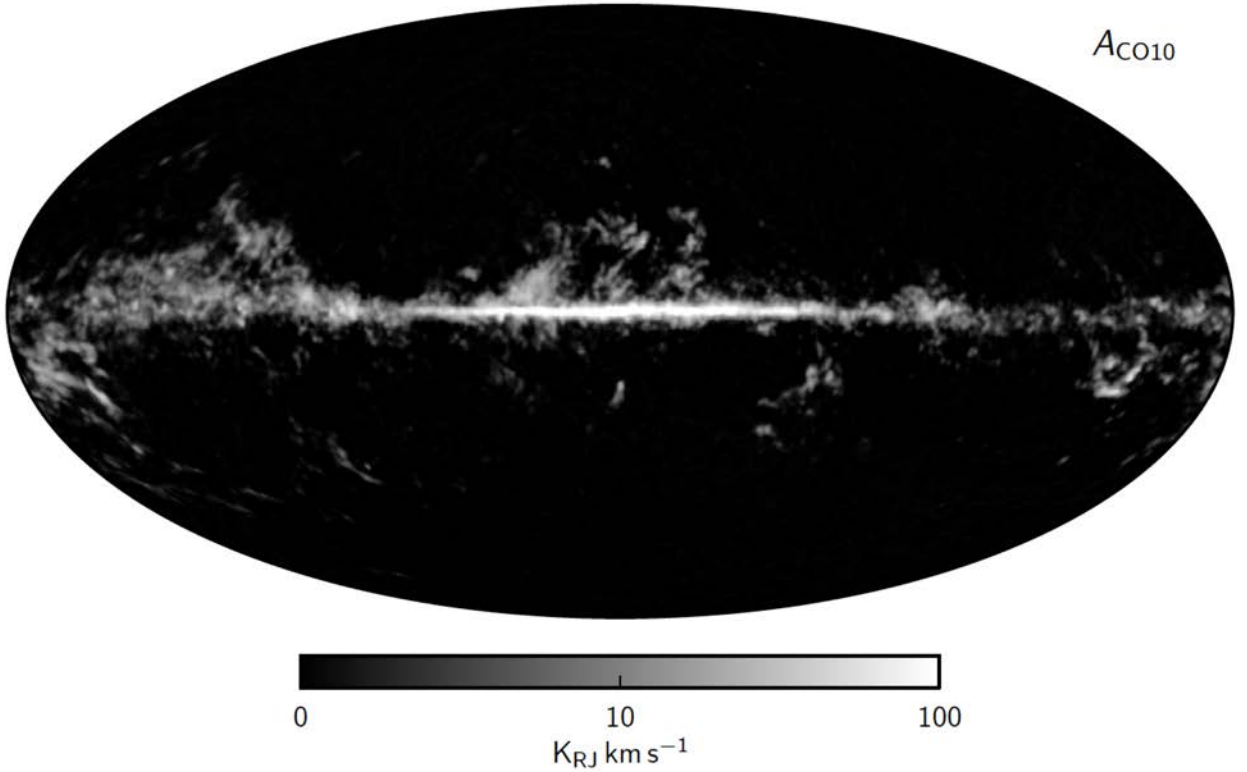


Planck 2015 results. X

# CO line emission

- Rotational transitions of carbon monoxide (CO) in the molecular cloud: CO rotation energy is quantized.
- The most effective tracer of molecular interstellar matter.
- Empirical relationship:

$$N(H_2) = 3\times10^{20}\int T_{b,\nu}(CO)du[cm^{-2}]$$

$$\Delta\nu_D = \frac{\nu_0}{c}\left(\frac{2kT}{m} + \upsilon_{turb}^2\right)^{1/2}$$

# Zodiacal light, Cosmic Infrared Background

- Inter Planetary dust (IPD) in our Solar system, concentrated within the orbit of Jupiter.

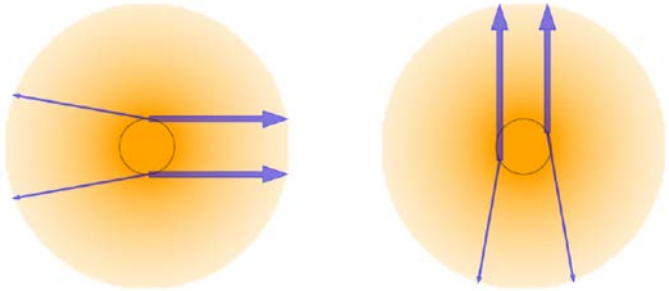

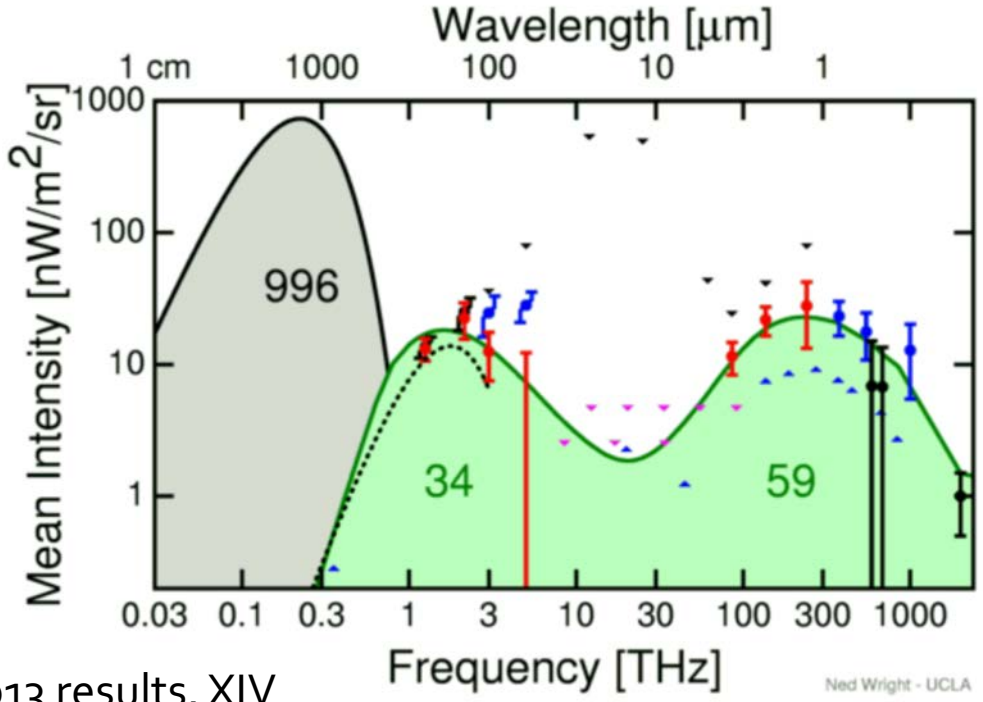


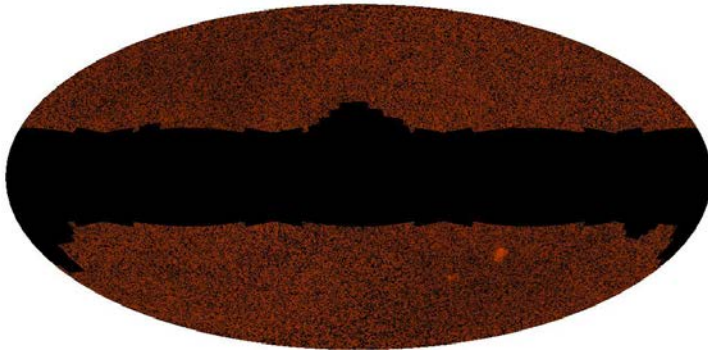

Planck 2013 results. XIV

# Component separation methods

- Template fitting
- Parametric methods:

  Commander
- Non-parametric method:

  Needlet Internal linear combination (NILC)

  Independent Component Analysis (FastICA)

  Spectral Matching Independent Component Analysis (SMICA).

  Analytical Blind  Separation ( ABS )

# Template fitting

- Assume sky at given pixel $\hat{n}$ and frequency $\nu$ is a superposition of various components and noise.

$$T(\hat{n}, \nu) = \sum_i \alpha_i(\nu) X_i(\hat{n}) + n(\hat{n}, \nu)$$

where $\alpha_i(\nu)$ is the template coefficients, the frequency dependence

- Then fit the combination of templates in a least-squares sense to the observation sky map
- WMAP: $$M(\nu, p) = c_1(\nu)[T_K(p) - T_{Ka}(p)] + c_2(\nu) I_{\mathrm{H}\alpha}(p) + c_3 M_{\mathrm{dust}}(p),$$

synchrotron template from lowest channels + free-free template from $H\alpha$ + dust template from Schlegel,Finkbeiner and Davis(SFD)

# Template fitting

## WMAP diffuse foreground templates

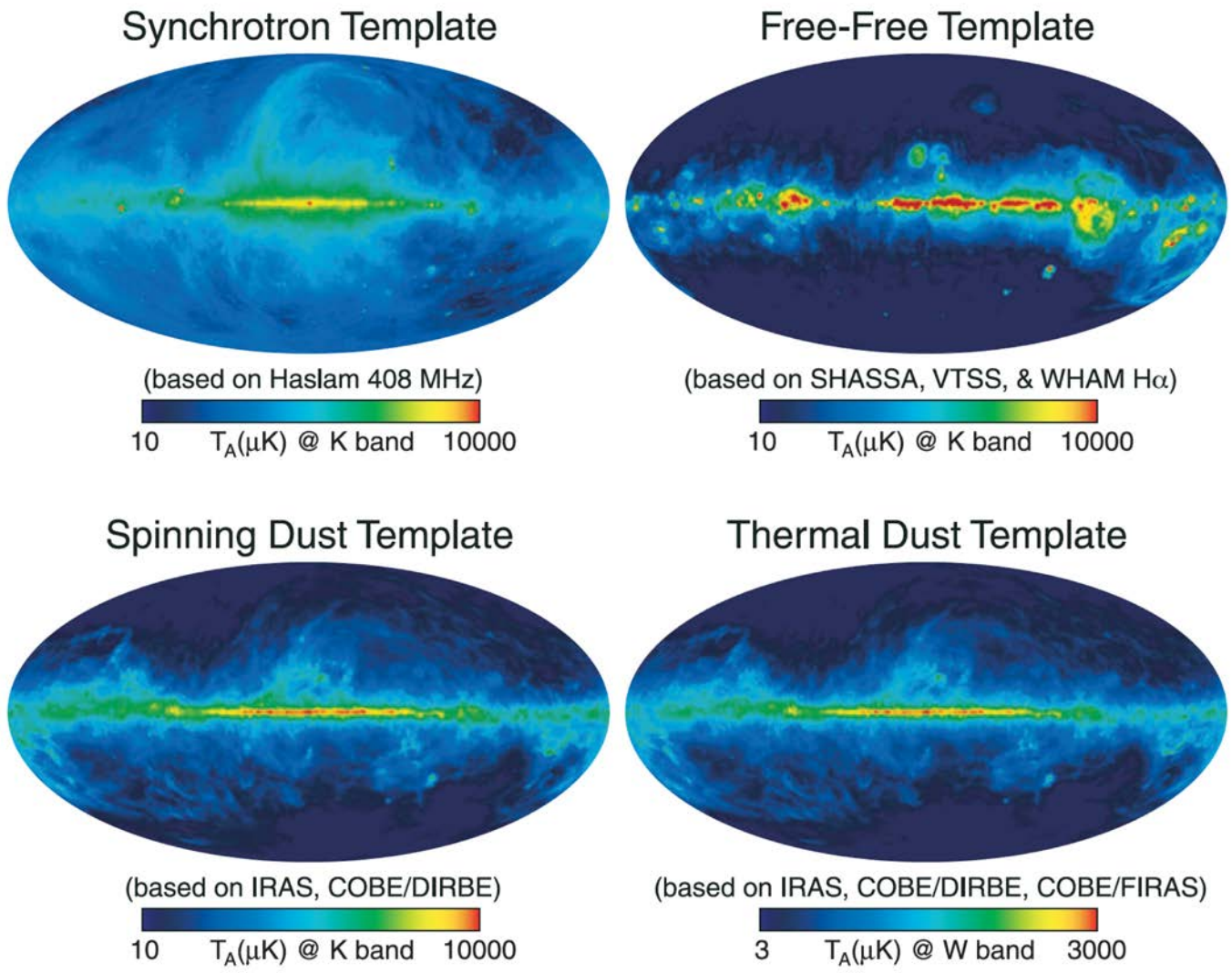


Bennett et al. (2013)

# Template fitting

- Templates are no need to be real physical components: SFD can represent both thermal dust at high frequencies and AME at low frequencies simultaneously
- Pros: statistical properties of noise in the foreground-cleaning map is unaffected
- Cons: assumes a separable nature for frequency and spatial positions, which is not true for real sky

  (spectral index of synchrotron emissions varies over the sky, and even have curvature)

# COMMANDER

- COMMANDER: Bayesian parametric pixel-by-pixel fitting with MCMC Gibbs sampling

- MCMC sampling(Metropolis-Hastings algorithm):

  if $\pi(\boldsymbol{x}_{i+1}) > \pi(\boldsymbol{x}_i)$, the proposed step is always accepted;

  otherwise, the step is accepted with probability $\pi(\boldsymbol{x}_{i+1})/\pi(\boldsymbol{x}_i)$

$$p_{\mathrm{acc}}(\boldsymbol{x}_{i+1}|\boldsymbol{x}_i) = \min\left[\frac{\pi(\boldsymbol{x}_{i+1})}{\pi(\boldsymbol{x}_i)}, 1.0\right]$$

- Gibbs sampling:

  When we sample multivariate probability distributions $p(\boldsymbol{x})$,

  start with $x^{(0)} = \left\{x_1^{(0)}, \ldots, x_d^{(0)}\right\}$,

  draw $x_1^{(1)}$ from $p(x_1|x_2^{(0)}, \ldots, x_d^{(0)})$, then $x_2^{(1)}$ from $p\left(x_2\middle|x_1^{(0)}, x_3^{(0)}, \ldots, x_d^{(0)}\right)$, etc

# COMMANDER

- The maximum of joint posterior distribution $P(\boldsymbol{s}, \boldsymbol{f}(\theta), C_l|\boldsymbol{d})$ can tell us the best fit parameter $\theta$ and CMB power spectrum $C_l$ ,

  where $\boldsymbol{s}$ is the signal, $\boldsymbol{f}(\theta)$ is the foreground, $\boldsymbol{d}$ is observed data.

- This is a very high-dimensional distribution, to study its characteristics, MCMC sampling is needed.
- But firstly, sampling joint pdf is difficult ,use Gibbs sampling

$$\{\mathbf{s}, \mathbf{f}\}^{(i+1)} \leftarrow P(\mathbf{s}, \mathbf{f}|C_\ell^{(i)}, \mathbf{d}),$$

$$C_\ell^{(i+1)} \leftarrow P(C_\ell|\mathbf{s}^{(i+1)}).$$

  to reduce the problem:  sampling two conditional density.

# COMMANDER

- Assuming the conditional distributions are Gaussian likelihoods, and using Bayes theorem

$$P(\mathbf{s}, \mathbf{f}|C_\ell^{(i)}, \mathbf{d}) \propto \exp\left(-\frac{1}{2}\sum_\nu (\mathbf{d}_\nu - \mathbf{s}_\nu - \mathbf{f}_\nu)^T \mathbf{N}_\nu^{-1} (\mathbf{d}_\nu - \mathbf{s}_\nu - \mathbf{f}_\nu)\right) \exp\left(-\frac{1}{2}\mathbf{s}^T \mathbf{S}^{-1} \mathbf{s}\right),$$

$$P(C_\ell|\mathbf{s}) \propto \exp\left(-\frac{1}{2}\mathbf{s}^T \mathbf{S}^{-1} \mathbf{s}\right) \propto \exp\left(-\frac{1}{2}(2\ell+1)\frac{\sigma_\ell^2}{C_\ell}\right),$$

- $\boldsymbol{N}_\nu$: noise covariance at frequency $\nu$

  $\boldsymbol{S}$ : signal covariance,
- Multivariate Gaussian $\sigma_\ell^2 = \sum_m |s_{\ell m}|^2/(2\ell+1)$ıa for $C_l$
- Simplify version of detailed $S_\nu + f_\nu$ parametric treatment:

$$(\mathbf{s} + \mathbf{f}) = s_{\rm CMB}(\hat{n}) + A_{\rm lf}(\hat{n})\left(\frac{\nu}{\nu_{0,\rm lf}}\right)^{\beta_{\rm lf}(\hat{n})} + A_{\rm CO}(\hat{n}) f_{\nu,\rm CO}$$

$$+ A_{\rm d}(\hat{n}) \frac{e^{h\nu_{0,\rm d}/kT_{\rm d}(\hat{n})} - 1}{e^{h\nu/kT_{\rm d}(\hat{n})} - 1}\left(\frac{\nu}{\nu_{0,\rm d}}\right)^{\beta_d(\hat{n})+1},$$

# summary of main parametric model

COMMANDER

| Component | Free parameters and priors | Brightness temperature, $s_\nu$ [$\mu K_{RJ}$] | Additional information |
|---|---|---|---|
| CMB[a] . . . . . | $A_{cmb} \sim \mathrm{Uni}(-\infty, \infty)$ | $x = \frac{h\nu}{k_B T_{CMB}}$<br>$g(\nu) = (\exp(x)-1)^2/(x^2\exp(x))$<br>$s_{CMB} = A_{CMB}/g(\nu)$ | $T_{CMB} = 2.7255$ K |
| Synchrotron[a] . . . | $A_s > 0$<br>$\alpha > 0$, spatially constant | $s_s = A_s \left(\frac{\nu_0}{\nu}\right)^2 \frac{f_s(\frac{\nu}{\alpha})}{f_s(\frac{\nu_0}{\alpha})}$ | $\nu_0 = 408$ MHz<br>$f_s(\nu) =$ Ext template |
| Free-free . . . . . | $\log \mathrm{EM} \sim \mathrm{Uni}(-\infty, \infty)$<br>$T_e \sim N(7000 \pm 500\,\mathrm{K})$ | $g_{ff} = \log\left\{\exp\left[5.960 - \sqrt{3}/\pi \log(\nu_9\ T_4^{-3/2})\right] + e\right\}$<br>$\tau = 0.05468\ T_e^{-3/2}\ \nu_9^{-2}\ \mathrm{EM}\ g_{ff}$<br>$s_{ff} = 10^6\, T_e\, (1 - e^{-\tau})$ | $T_4 = T_e/10^4$<br>$\nu_9 = \nu/(10^9\,\mathrm{Hz})$ |
| Spinning dust . . . | $A^1_{sd}, A^2_{sd} > 0$<br>$\nu^1_p \sim N(19 \pm 3\,\mathrm{GHz})$<br>$\nu^2_p > 0$, spatially constant | $s_{sd} = A_{sd} \cdot \left(\frac{\nu_0}{\nu}\right)^2 \frac{f_{sd}(\nu \cdot \nu_{p0}/\nu_p)}{f_{sd}(\nu_0 \cdot \nu_{p0}/\nu_p)}$ | $\nu^1_0 = 22.8$ GHz<br>$\nu^2_0 = 41.0$ GHz<br>$\nu_{p0} = 30.0$ GHz<br>$f_{sd}(\nu) =$ Ext template |
| Thermal dust[a] . . | $A_d > 0$<br>$\beta_d \sim N(1.55 \pm 0.1)$<br>$T_d \sim N(23 \pm 3\,\mathrm{K})$ | $\gamma = \frac{h}{k_B T_d}$<br>$s_d = A_d \cdot \left(\frac{\nu}{\nu_0}\right)^{\beta_d+1} \frac{\exp(\gamma\nu_0)-1}{\exp(\gamma\nu)-1}$ | $\nu_0 = 545$ GHz |
| SZ . . . . . | $y_{sz} > 0$ | $s_{sz} = 10^6\, y_{sz}/g(\nu)\, T_{CMB} \left(\frac{x(\exp(x)+1)}{\exp(x)-1} - 4\right)$ | |
| Line emission . . | $A_i > 0$<br>$h_{ij} > 0$, spatially constant | $s_i = A_i h_{ij} \frac{F_i(\nu_j)}{F_i(\nu_0)} \frac{g(\nu_0)}{g(\nu_j)}$ | $i \in \begin{cases} \mathrm{CO}\ J=1\to0 \\ \mathrm{CO}\ J=2\to1 \\ \mathrm{CO}\ J=3\to2 \\ 94/100 \end{cases}$<br>$j =$ detector index<br>$F =$ unit conversion |

Planck 2015 results. X

# COMMANDER

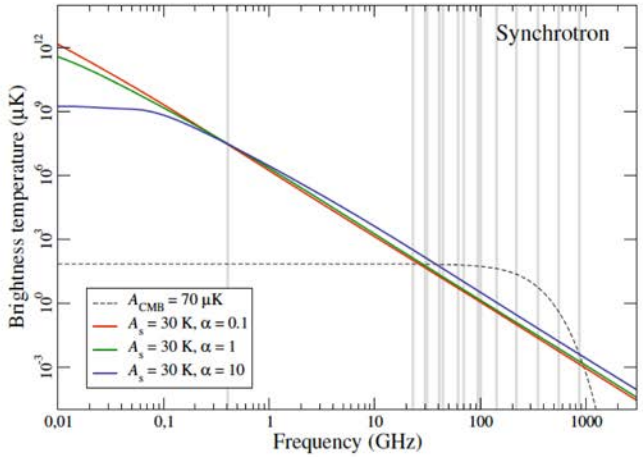


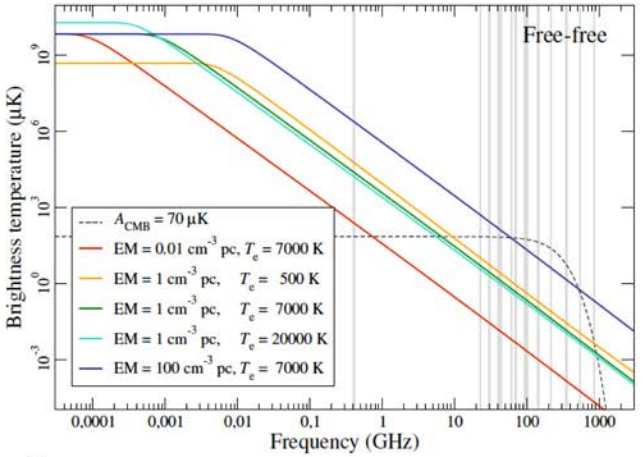


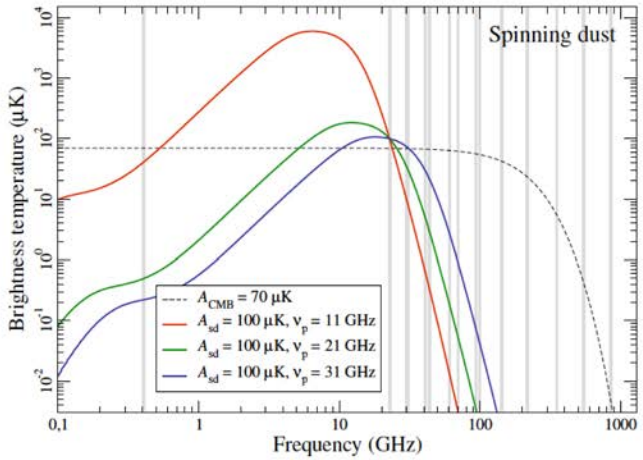


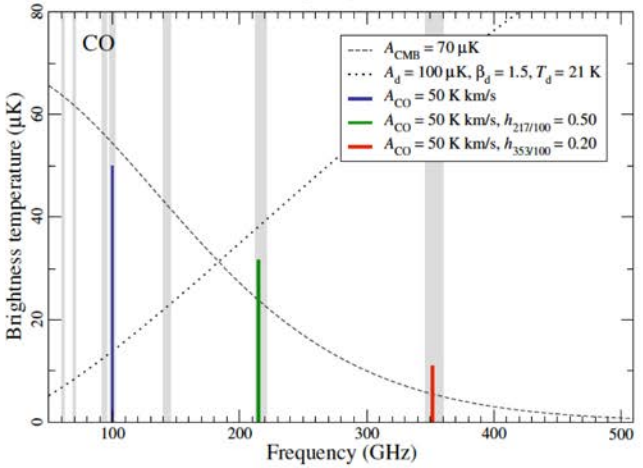


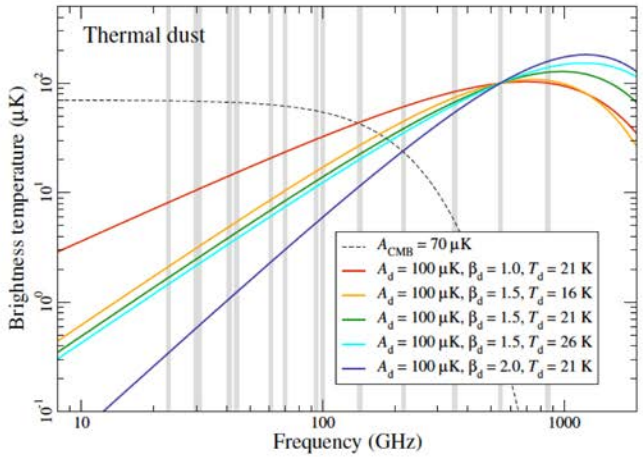


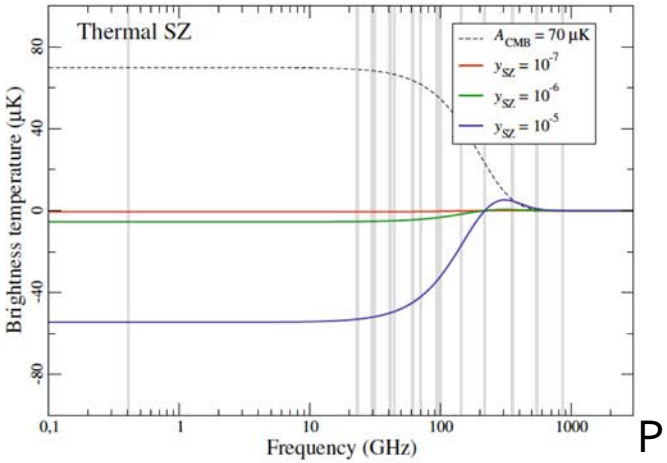


Planck 2015 results. X

# COMMANDER

- Pros:

  best estimate of the power spectrum with posterior probability

  best estimate of foreground parameters with errors

  component separation method

  can apply our knowledge of physical processes and additional observational constrain as priors

- Cons:

  sensitive to the assumed priors on the foreground model parameters

  computationally intensive, so the resolution is the lowest (though the high resolution may not be necessary for inflationary B-mode detection on large scale)

# NILC

- Minimum-variance internal linear combination in needlet space.

- Advantage of spherical needlets over spherical harmonics :

spherical harmonics are global functions, suffers from Gibbs phenomenon

needlets are localized at a certain region and a finite number of frequencies, also decay quasi-exponentially

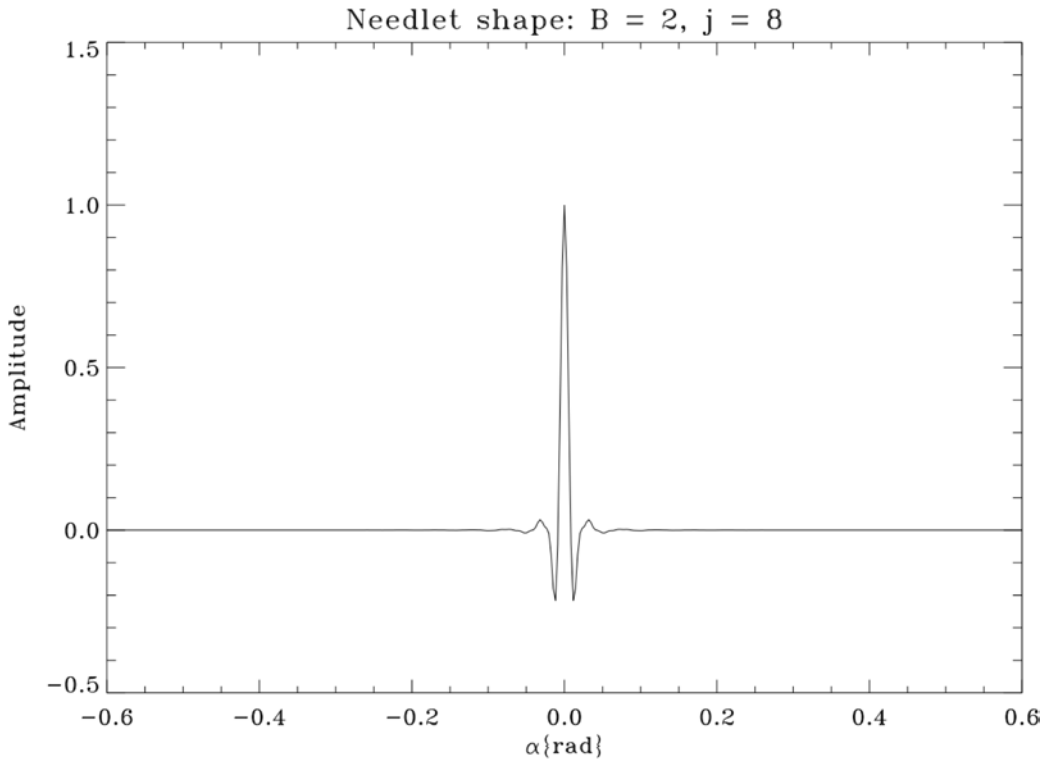


D.Marinucci et al. (2018)

# NILC

- Main idea:

  signal and foregrounds are uncorrelated +

  signal is the same in every maps +

  foreground components are canceled out

  $\Longrightarrow$ linearly combined map have the total minimum variance

- Pros:

  Localization in pixel space allows the weight to adapt local conditions.

  Localization in harmonic space allows to reject foreground on large scales and noise on small scales.

- Cons:

  Relies on the independence between signal and foreground, can not separate each Galactic foreground component

# NILC

- Detection contains CMB signal and contamination

$$x_\nu = a_\nu\, s + n_\nu \qquad a_\nu \equiv dB_\nu(T)/dT|_{T=T_{\rm CMB}}$$

- Estimate signal as weighted internal linear combination

$$\widehat{s} = \sum_\nu w_\nu\, x_\nu \qquad \sum_\nu w_\nu\, a_\nu = 1$$

- to be of minimum variance

$$\frac{\partial \left\langle \widehat{s}^{\,2} \right\rangle}{\partial\, w_\nu} \equiv \frac{\partial}{\partial\, w_\nu} \left( \sum_{\nu'} \sum_{\nu''} w_{\nu'}\, \mathrm{C}_{\nu'\nu''}\, w_{\nu''} \right) = 0$$

Where $\mathrm{C}_{\nu\nu'}(p) = \dfrac{1}{N_p} \displaystyle\sum_{p' \in \mathcal{D}(p)} x_\nu(p') x_{\nu'}(p')$

is the covariance matrix average over a certain domain surrounding pixel p.

# NILC

$$\widehat{s} = s + \sum_{\nu} w_{\nu}\, n_{\nu}$$

Unbiased estimate of CMB and minimized residual foreground

- Solution: the resulting weight to meet the minimum variance

$$\widehat{\omega}^{c}_{jk} = \frac{\sum_{c'} \left[\widehat{R}^{-1}_{jk}\right]^{cc'} a^{c'}}{\sum_{c} \sum_{c'} a^{c} \left[\widehat{R}^{-1}_{jk}\right]^{cc'} a^{c'}} \qquad \sum_{c=1}^{n_c} a^{c}\, \omega^{c}_{jk} = 1$$

- $c$: frequency channel $i$: scale $k$: pixel
- Needlet coefficient: $\beta^{X}_{jk} = \int_{S^2} X(\hat{n})\, \Psi_{jk}(\hat{n})\, \mathrm{d}\Omega_{\hat{n}}$
- Covariance matrix: average of product over some space domain

$$R^{cc'}_{jk} = \langle \beta^{c}_{jk} \beta^{c'}_{jk} \rangle$$

- Reconstruction :

$$\beta^{\mathrm{NILC}}_{jk} = \sum_{c=1}^{n_c} \omega^{c}_{jk}\, \beta^{X,c}_{jk}$$

# FastICA

- The ICA (independent component analysis) model is given by

$$x^j(\hat{n}_i) = A_k^j s^k(\hat{n}_i)$$

$j$: frequency, $A$: mixing matrix , $s^k$ : signal including foregrounds

- Assume signal components are independent, then for

$$\mathbf{y}^k \equiv y^k(\hat{n}_i) = W_j^k x^j(\hat{n}_i)$$

we can find a $W_j^k$ to maximize the independency of $\boldsymbol{y}^k$.

- Which is equivalent to maximize non-Gaussianity.
- Key point is to find a suitable measure of non-Gaussianity of $\boldsymbol{y}^k$

- Need no assumption about the spatial distribution and frequency dependence of foreground components
- Many application in COBE, BEAST, WMAP, 21cm map, CO map in PLANCK

# SMICA

- Power spectra fitting approach in harmonic space, also no need of prior assumption of foreground

$$\mathbf{C}_\ell(\theta) = \mathbf{a}\mathbf{a}^\dagger C_\ell^{\mathrm{CMB}} + \mathbf{A}\mathbf{P}_\ell\mathbf{A}^\dagger + \mathbf{N}_\ell$$

here $\boldsymbol{C}_l(\theta)$ is the cross band power with $\theta$ contains whatever parameters are needed to determine the model above.

$\boldsymbol{a}$ : CMB spectrum, $\boldsymbol{A}$ : foreground spectrum,

$\boldsymbol{P}_l$: foreground covariance matrix , $\boldsymbol{N}_l$: diagonal noise matrix

- Sample spectral covariance matrix $\hat{\mathbf{C}}_\ell = \frac{1}{2\ell+1}\sum_m \mathbf{x}_{\ell m}\mathbf{x}_{\ell m}^\dagger$
- Best-fit parameters $\theta$:

$$\hat{\theta} = \arg\min_\theta \sum_\ell (2\ell+1)\left(\hat{\mathbf{C}}_\ell \mathbf{C}_\ell(\theta)^{-1} + \log\det \mathbf{C}_\ell(\theta)\right)$$

equivalent to maximizing the likelihood under condition that they follow Gaussian isotropic distribution characterized by the spectra and cross band matrix.

# SMICA

- Get the CMB power spectrum

$$\hat{a}_{\ell m}^{\mathrm{CMB}} = \mathbf{w}_{\ell}^{\dagger}\mathbf{x}_{\ell m}$$

where:

$$\mathbf{w}_{\ell} = \frac{\mathbf{C}_{\ell}(\theta)^{-1}\mathbf{a}}{\mathbf{a}^{\dagger}\mathbf{C}_{\ell}(\theta)^{-1}\mathbf{a}}$$

- SMICA can not blindly separate the components with similar angular power spectrum

  Fortunately, CMB's is distinct with other foregrounds'

  But component separation between foreground can be difficult (same with NICL)

# ABS

- Analytical method of blind separation on harmonic space
- Based on PJ Zhang, J. Zhang, L. Zhang; arxiv:1608.03707 and Jian Yao, Le Zhang, Yuxi Zhao, et al; arxiv:1807.07016
- Cross band power spectrum

$$\mathcal{D}_{ij}^{\rm obs}(\ell) = f_i f_j \mathcal{D}^{\rm cmb}(\ell) + \mathcal{D}_{ij}^{\rm fore}(\ell) + \delta\mathcal{D}_{ij}^{\rm noise}(\ell)$$

- $D_{ij}^{fore}$ has order of frequency channel number $N_f$, but rank $M$ depends on the number of independent foreground
- Without noise + $M < N_f$ , there is unique analytical solution of $D^{cmb}$. Achieved by Sylvester's determinant theorem.
- $$\mathcal{D}_{\rm B} = \left( \sum_{\mu=1}^{M+1} G_\mu^2 \lambda_\mu^{-1} \right)^{-1}$$

$\mu$-th eigenvector of $D_{ij}$ is $\boldsymbol{E}^{(\mu)}$

$$G_\mu \equiv \mathbf{f}^{\rm B} \cdot \mathbf{E}^{(\mu)}$$

# ABS

- In the case with noise: normalize the data + discard the eigenvector that is dominated by the noise
- $\left\langle \left(\delta D_{ij}^{noise}\right)^2 \right\rangle = \sigma_{D,i}^{noise} \sigma_{D,j}^{noise} (1 + \delta_{ij})/2$

$$\tilde{\mathcal{D}}_{ij}^{\rm obs} \equiv \frac{\mathcal{D}_{ij}^{\rm obs}}{\sqrt{\sigma_{\mathcal{D},i}^{\rm noise}\sigma_{\mathcal{D},j}^{\rm noise}}} + \tilde{f}_i \tilde{f}_j \mathcal{S}\,,$$

$$\tilde{f}_i \equiv \frac{f_i}{\sqrt{\sigma_{\mathcal{D},i}^{\rm noise}}}\,, \quad \tilde{G}_\mu \equiv \tilde{\mathbf{f}} \cdot \tilde{\mathbf{E}}^\mu\,,$$

- Then only use eigenmodes with $\lambda_\mu >$ noise level

$$\hat{\mathcal{D}}^{\rm cmb} = \left( \sum^{\tilde{\lambda}_\mu \geq \lambda_{\rm cut}} \tilde{G}_\mu^2 \tilde{\lambda}_\mu^{-1} \right)^{-1} - \mathcal{S}$$

- $S$ is a free parameter to reduce the systematic error and stabilize the computation

# ABS

- Resulting eigenvalue

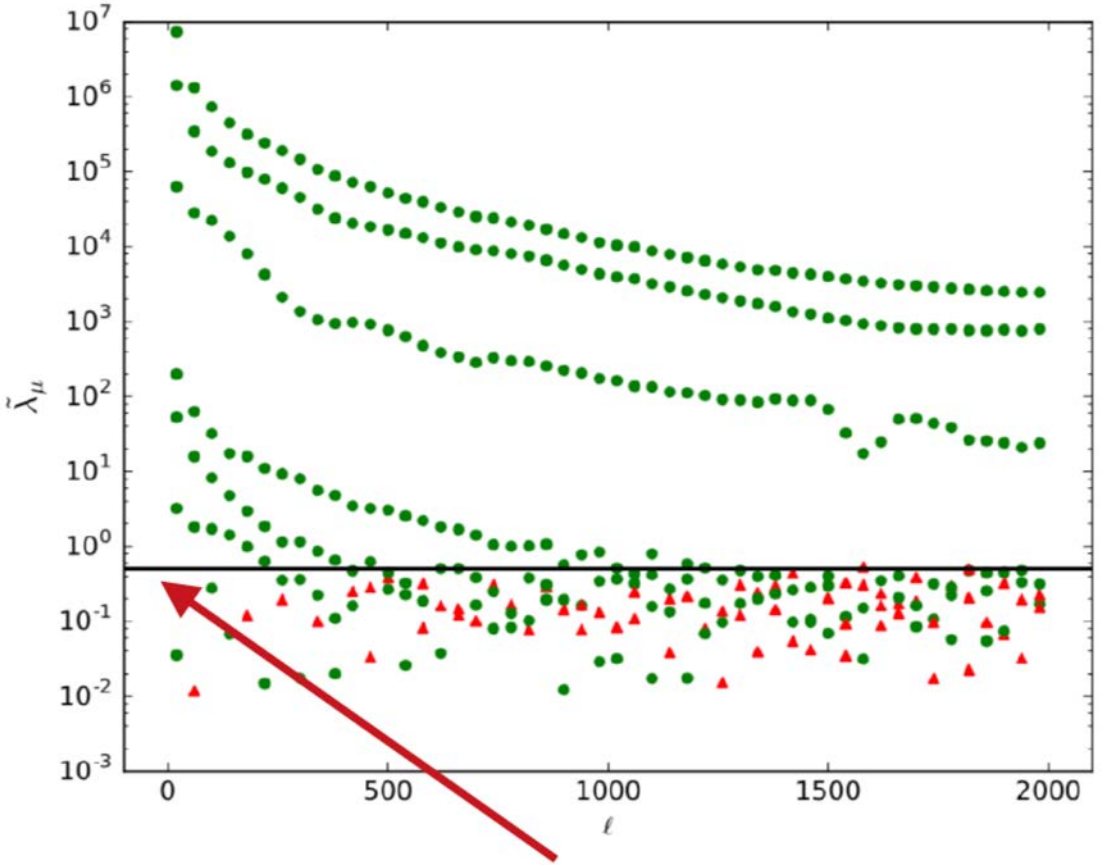


eigenmodes below 1/2 excluded, which are essentially noise-dominated modes

Yao et al. (2018)

# ABS

- Resulting eigenvector, a mixture of several astrophysical components

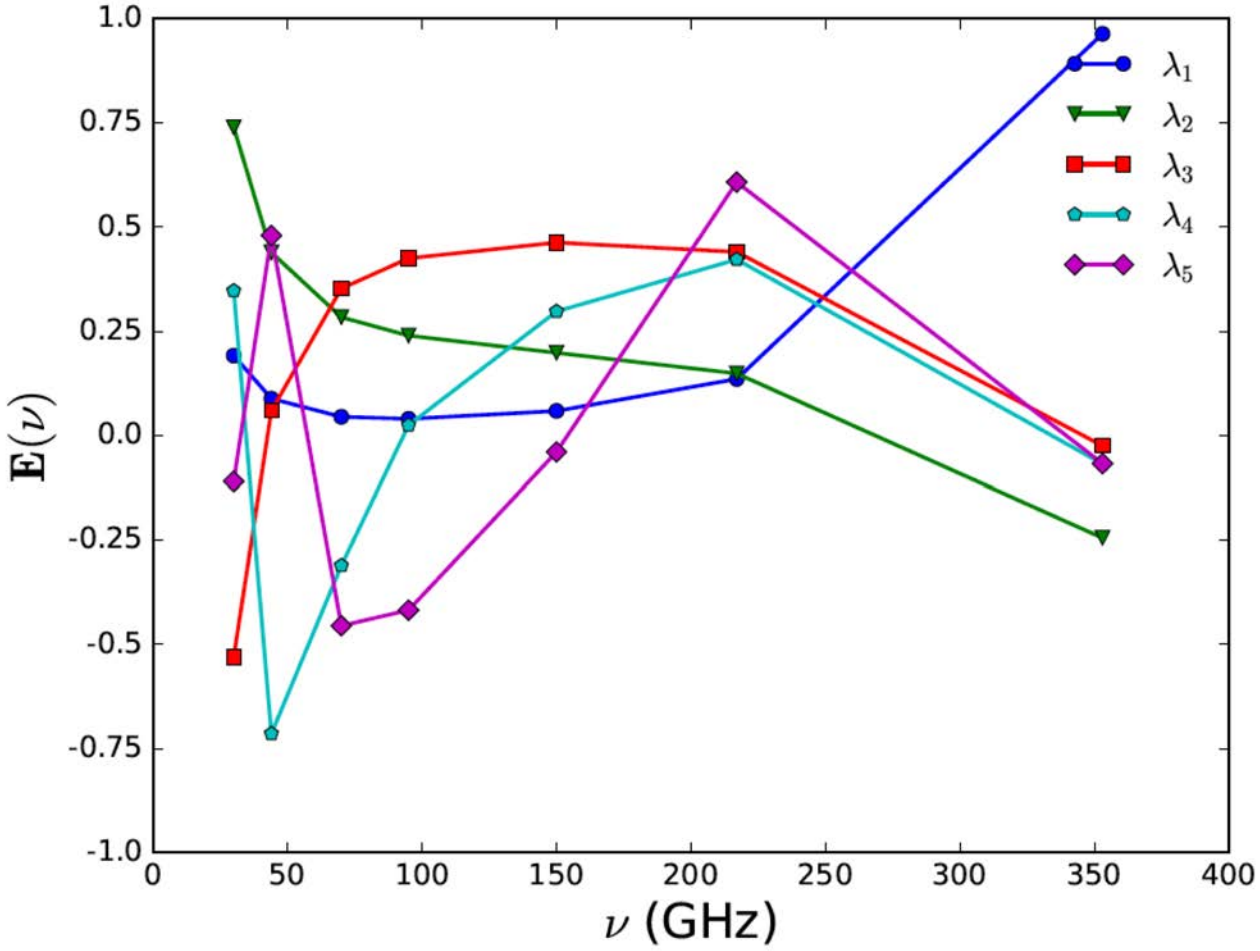


- The other two eigenvectors are noise dominated

Yao et al. (2018)

# ABS

- Recovered CMB power spectrum

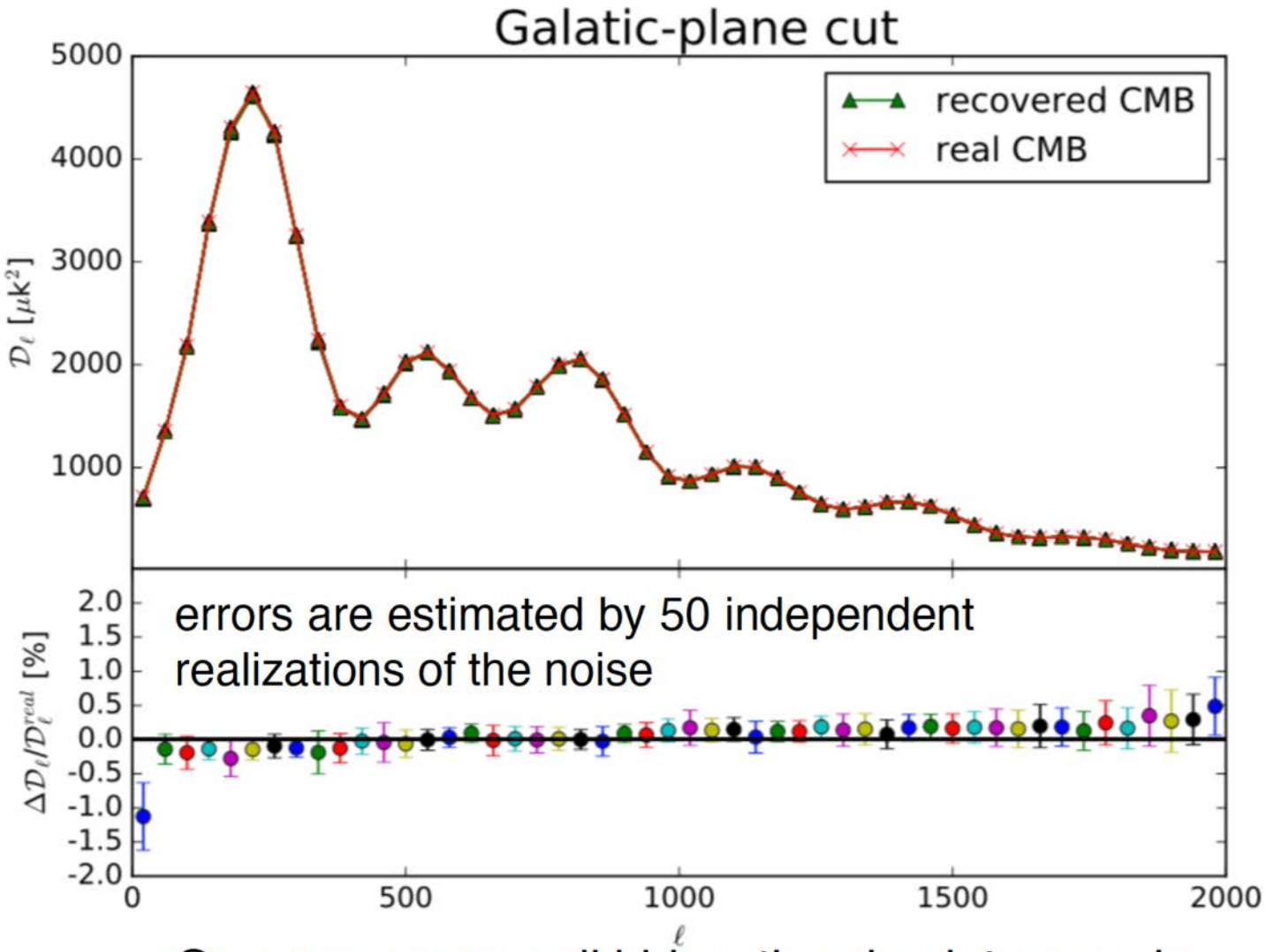


On average over all l-bins, the absolute error is about –0.56 μK² with 1-σ error of 2.66 μK².

Yao et al. (2018)

# ABS

- Robustness test:
  reverse the mask

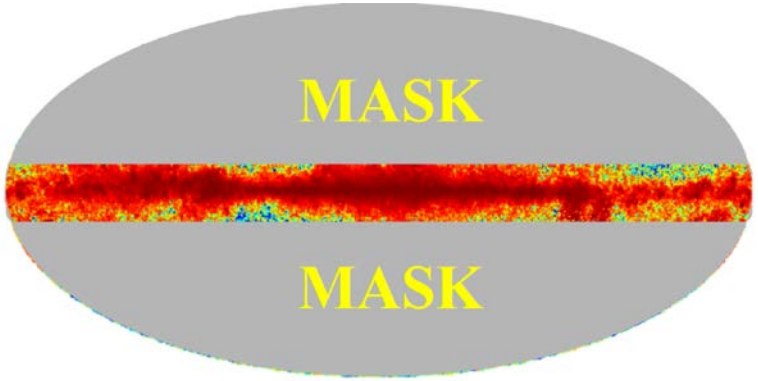


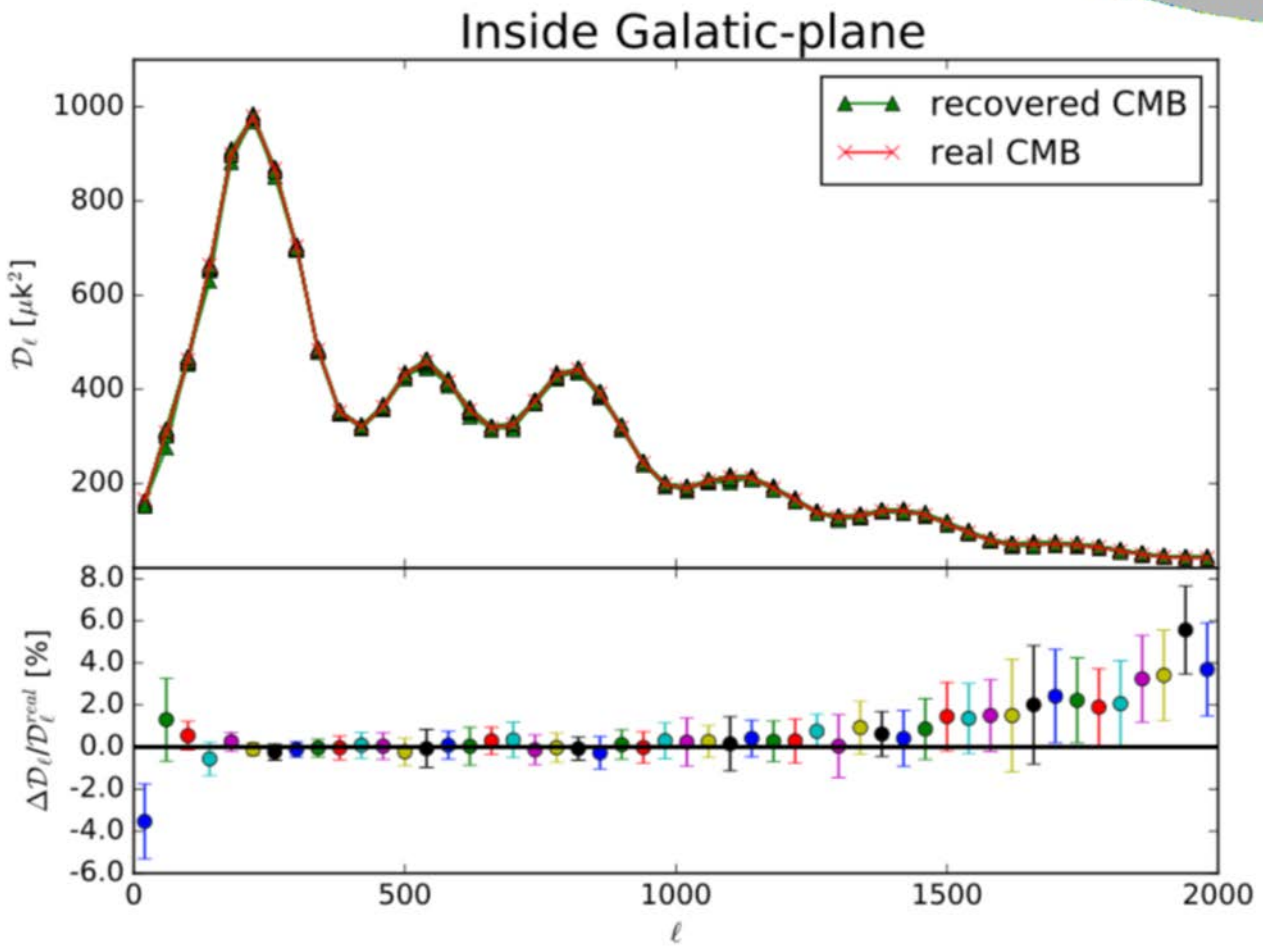


- still have <1% deviation on average

Yao et al. (2018)

# ABS

- Using simulation sky maps, so  real-world instrument effects : beam shape, correlated non-Gaussian noise may affected the result
- Additional complex foreground and point sources may complicate the removal process

# Thanks!

# Q&A